Quasi-Parallel Flows – Lubrication Approximation

8

A significant number of practically important flows (application of coatings or paints, lubrication flows between tight-fitting parts, liquid jets, etc.) have streamlines which are almost parallel. We discuss first (Section 8.1) the so-called lubrication approximation, which allows us to perform a theoretical calculation for these flows, and we give several examples of flows between two solid surfaces. We use then the same method (Section 8.2) to deal with fluid films which have a free surface: we treat specifically problems of wetting, dynamic contact angle and analyze the spreading of liquid layers or droplets. A particularly interesting case is that of Marangoni effects, where the flow results from spatial variations of the surface tension at the interface. Finally, we discuss a similar problem involving the drop of a viscous jet and the Rayleigh-Plateau instabilities which can appear, and which occur because of surface tension (Section 8.3).

8.1 Lubrication approximation

8.1.1 Quasi-parallel flows

We have discussed in Chapter 4 one-dimensional flows for which only one component of the velocity does not vanish. In this case, the non-linear term $(\mathbf{v} \cdot \nabla)\,\mathbf{v}$ of the Navier-Stokes equation vanishes identically, because the gradient of the velocity $\mathbf{v}$ is normal to it. We then end up with a linear equation of motion for the fluid (Equation 4.59) which applies whatever the Reynolds number of the flow might be (so long as instabilities do not appear).

In this chapter, we study flows for which the streamlines are almost parallel, such as, for example, flows between solid walls which are at a very small angle θ to each other, or flows in a thin liquid layer. We can then neglect the non-linear terms, but only if certain specific conditions are satisfied by the Reynolds number: in that case, we speak of the *lubrication approximation*.

Later on, in Chapter 9, we discuss flows with arbitrary geometries: in that case, the condition on the Reynolds number for being able to neglect non-linear terms, is even more stringent ($Re \ll 1$).

We encounter quasi-parallel flows in a number of applications such as the spreading of a fluid film, or the lubrication of rotating machinery. We can thus calculate the dynamics of the spreading of a film in the former case, or the forces between the moving surfaces in the latter, by making the assumption that the flows are effectively parallel to the surfaces of these films.

Physical Hydrodynamics. Second Edition. Etienne Guyon *et al.*

8.1.2 Assumptions of the lubrication approximation

We assume that we have an angle $\theta \ll 1$ at all points between the walls, so that the characteristic distances over which flow parameters change are everywhere much greater than their separation, as shown in Figure 8.1. In the following, we consider a two-dimensional configuration where only the x- and y-directions are involved, but these results can be easily generalized to a three-dimensional case.

Let us find out what becomes of the different terms of the Navier-Stokes equation (Equation 4.30) for two-dimensional flow in the x-y plane. As we have previously indicated (Section 4.2.2), the flow does not result only from the pressure gradient, but from that of the combination $(p - \rho \mathbf{g}\cdot\mathbf{r})$, where $\mathbf{r}$ is the radius-vector for the point in question. In order to simplify the writing, we assume that ∇p, in fact, denotes $\nabla(p - \rho \mathbf{g}\cdot\mathbf{r})$. The components of Equation 4.30 then become:

$$\frac{\partial v_x}{\partial t} + (\mathbf{v}.\nabla)\, v_x = -\frac{1}{\rho}\frac{\partial p}{\partial x} + \nu\left(\frac{\partial^2 v_x}{\partial x^2} + \frac{\partial^2 v_x}{\partial y^2}\right) \tag{8.1a}$$

and:

$$\frac{\partial v_y}{\partial t} + (\mathbf{v}.\nabla)\, v_y = -\frac{1}{\rho}\frac{\partial p}{\partial y} + \nu\left(\frac{\partial^2 v_y}{\partial x^2} + \frac{\partial^2 v_y}{\partial y^2}\right). \tag{8.1b}$$

We must add to this equation the condition for conservation of mass for an incompressible fluid, i.e. $\nabla\cdot\mathbf{v} = 0$:

$$\frac{\partial v_x}{\partial x} + \frac{\partial v_y}{\partial y} = 0. \tag{8.2}$$

We first consider a stationary flow, which allows us to neglect terms such as $\partial/\partial t$, and we carry out the discussion based on an approximate evaluation of the orders of magnitude of the different terms. In the case of a stable and slow *laminar* flow, we observe experimentally that the trajectories of the fluid particles follow the surface of the walls, as shown in Figure 8.1. Therefore, in the middle of the flow, we can assume that the angle between the velocity and the wall $y = 0$ is of the order of the angle θ ($\ll 1$) between the two walls, so that:

$$v_y \approx v_x\, \theta \approx U\theta, \tag{8.3}$$

where U is the characteristic velocity of the flow (e.g., the average velocity or even the maximum velocity at the center of the channel, both of which can be considered to be of the same order of magnitude in terms of the approximation that we are carrying out). Considering that we are assuming a Poiseuille-type velocity profile between the walls, we can consider that the typical distance, over which variations of the velocity in the y-direction occur, is the local thickness $e(x)$, which we will assume to have a typical value e_0 (this amounts to saying that the relative change in the thickness is small along the length L). We thus obtain:

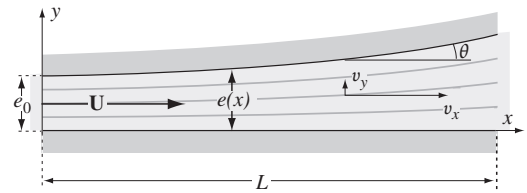

Figure 8.1 *Schematic diagram of the geometry of a lubrication flow*

$$\frac{\partial v_x}{\partial y} \approx \frac{U}{e_0} \qquad \text{(8.4a)} \qquad \text{and:} \qquad \frac{\partial v_y}{\partial y} \approx \frac{U\,\theta}{e_0}, \qquad \text{(8.4b)}$$

from which, using Equations 8.2:

$$\frac{\partial v_x}{\partial x} = -\frac{\partial v_y}{\partial y} \approx \frac{U\,\theta}{e_0} \qquad (8.5)$$

(the orders of magnitude are specified in terms of their absolute values). Using the above results, we estimate in the same way the second derivatives:

$$\frac{\partial^2 v_x}{\partial x\,\partial y} \approx \frac{U\theta}{e_0^2}, \qquad \text{(8.6a)} \qquad \frac{\partial^2 v_x}{\partial y^2} \approx \frac{U}{e_0^2} \qquad \text{(8.6b)}$$

and:

$$\frac{\partial^2 v_y}{\partial y^2} \approx \frac{U\,\theta}{e_0^2}. \qquad (8.6c)$$

We also state an upper limit for the absolute value of the terms $\partial^2 v_x/\partial x^2$ and $\partial^2 v_y/\partial x \partial y$ (which are opposite to each other because of the incompressibility condition) by taking $\partial/\partial x \approx 1/L$; this leads to:

$$\frac{\partial^2 v_x}{\partial x^2} = -\frac{\partial^2 v_y}{\partial x \partial y} \approx \frac{U\,\theta}{e_0\,L} \qquad \text{(8.7a)} \qquad \text{and, similarly:} \qquad \frac{\partial^2 v_y}{\partial x^2} \approx \frac{U\,\theta}{L^2}. \qquad \text{(8.7b)}$$

These terms are therefore very small relative to the second derivatives with respect to y; the latter will therefore be the only viscosity terms retained in Equations 8.1a and 8.1b.

Let us now consider the conditions under which the non-linear term of the component of the equation of motion, in the direction of the average flow, is negligible relative to the viscosity term. By using the previous results, we obtain:

$$v_x \frac{\partial v_x}{\partial x} \approx \frac{U^2\,\theta}{e_0}, \qquad \text{(8.8a)} \qquad v_y \frac{\partial v_x}{\partial y} \approx \frac{U^2\,\theta}{e_0} \qquad \text{(8.8b)} \qquad \text{and} \quad \nu \frac{\partial^2 v_x}{\partial y^2} \approx \frac{\nu\,U}{e_0^2}. \qquad \text{(8.8c)}$$

The non-linear terms are therefore negligible if:

$$\frac{U^2\,\theta}{e_0} \ll \nu \frac{U}{e_0^2}, \qquad \text{(8.9a)} \qquad \text{i.e.:} \qquad Re = \frac{U\,e_0}{\nu} \ll \frac{1}{\theta}. \qquad \text{(8.9b)}$$

For flows in arbitrary geometry, the condition obeyed by the Reynolds number, in order to be able to neglect the non-linear terms, is $Re \ll 1$. Equations 8.9b is then much less restrictive because in the lubrication geometries the angle θ is small relative to 1. We can thus continue to use a linear equation even for flows which correspond to a Reynolds number Re significantly greater than 1. In the limiting case of a parallel flow, the non-linear term vanishes at all values of the Reynolds number.

Let us calculate the component $\partial p/\partial y$ of the pressure gradient in the direction normal to the average flow on the basis of Equations 8.1b. We estimate, as in the previous case:

$$v_x \frac{\partial v_y}{\partial x} \approx \frac{U^2\,\theta}{L}, \qquad \text{(8.10a)} \quad v_y \frac{\partial v_y}{\partial y} \approx \frac{U^2\,\theta^2}{e_0}, \qquad \text{(8.10b)} \qquad \nu \frac{\partial^2 v_y}{\partial y^2} \approx \nu \frac{U\,\theta}{e_0^2}. \qquad \text{(8.10c)}$$

The viscous term resulting from Equations 8.10c is thus smaller by an order of magnitude in θ than that given by Equations 8.8c. If $Re \ll 1/\theta$ and e_0/L is sufficiently small, the non-linear terms in Equations 8.10a and 8.10b will be smaller than the viscous term in Equations 8.10c and, in any case, very small, in comparison with the viscous term of the equation, in the x-direction. We can thus consider that the pressure gradient transverse to the flow is zero (or, more precisely, that it reduces to the hydrostatic pressure) when θ is small, and the Reynolds number sufficiently small.

We should, however, note that this entire discussion assumes that there is a fully developed unperturbed laminar flow. Beyond certain critical flow velocities, even if Equation 8.9b is satisfied, the flow between parallel planes becomes unstable, and significant velocity components, normal to the average flow, appear. The preceding results are then no longer valid.

8.1.3 Non-stationary effects

Let us now go back to Navier-Stokes equation, written as in Equation 8.1, and assume that the flow changes over a characteristic time T, or that it is periodic with angular frequency ω (a parameter better suited for a periodic flow). The term $\partial\mathbf{v}/\partial t$ will then be either of order U/T or, equivalently, of $U\omega$. It will be negligible relative to the viscosity term if $|\partial\mathbf{v}/\partial t| \ll |\nu\,\boldsymbol{\nabla}^2\mathbf{v}|$, i.e.:

$$\frac{U}{T} \ll \nu\frac{U}{e_0^2} \qquad \text{or} \qquad Nt_\nu = \frac{e_0^2}{\nu T} \ll 1.$$

The ratio Nt_ν of the characteristic times appeared already in Equation 4.95 during our discussion of alternating flows between two planes (Section 4.5.4). The condition $Nt_\nu \ll 1$ expresses that the characteristic time e_0^2/ν for the diffusion of the velocity gradients (or of the vorticity) over the thickness e_0 of the fluid film is much smaller than the characteristic time T for the evolution of the flow or, equivalently, small compared to $1/\omega$. One notes that e_0^2/ν represents also the time needed to establish a stationary velocity profile: if the above condition is satisfied, the flow can then be considered as quasi-stationary, and the terms of the type $\partial\mathbf{v}/\partial t$ can be neglected.

8.1.4 Equations of motion in the lubrication approximation

In this case, if instabilities do not appear in the flow, and the conditions $\theta \ll 1$ and $Re \ll 1/\theta$ are satisfied, Equations 8.1a and 8.1b simplify, for a steady state flow, to:

$$\frac{1}{\rho}\frac{\partial p}{\partial x} = \nu\frac{\partial^2 v_x}{\partial y^2} \qquad (8.11a) \qquad \text{and:} \qquad \frac{\partial p}{\partial y} = 0, \qquad (8.11b)$$

which represents exactly the same system of equations as for a parallel flow. The velocity v_x will vary in the x-direction if the thickness is no longer a constant, but this variation will be much slower than in the y-direction, for which the characteristic distance for change is e_0. In order to calculate the velocity profile, we then integrate Equation 8.11a relative to y, as though $\partial p/\partial x$ were a constant (the x and y variables become decoupled). In effect, if the requirements for the lubrication approximation are satisfied, $\partial p/\partial x$ is practically independent of y, just as for a parallel flow; on the other hand, it varies, in the x-direction, over distances which are much larger than the thickness e_0 of the fluid layer. Weakly non-stationary flows can be treated in the same manner if the time-dependent change

in the velocity is sufficiently slow. We will see, further down, examples where the lack of stationarity plays a significant role.

8.1.5 An example of the application of the equation for lubrication: stationary flow between two moving planes making a small angle to each other

If we let a sheet of paper slide parallel to the horizontal surface of a smooth table, the presence of a film of air between the table and the sheet helps the sliding; on the other hand, if the sheet of paper has a few holes in it, it slides very poorly because there no longer exists a pressure difference between the outside air and this intermediate sheet. The pressure difference which exists in the former case is due to the formation of a wedge toward the back between the sheet and the table, shown schematically in Figure 8.2.

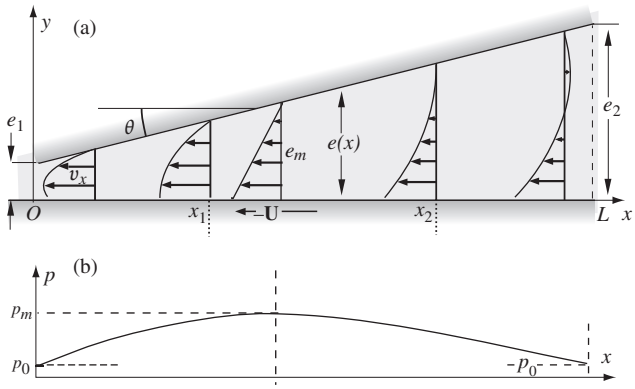

Figure 8.2 *Schematic diagram of the flow resulting from the motion of an inclined plane moving relative to a fixed horizontal plane; (a) the velocity field is shown in the reference frame in which the inclined plane is fixed; (b) variation of the pressure in the region between the two planes*

For this calculation, we will assume that the sheets extend infinitely in the transverse z-direction (perpendicular to the plane of the figure). Also, we will compute values of the force, and of the flow rate, which correspond to a layer of unit depth in that direction. Moreover, we change the reference frame and assume that the velocity of the sheet is zero, and that the lower plane is moving with a velocity **–U**; this allows us to obtain a stationary flow profile, because the lower surface moves in its own plane and the thickness of the fluid is therefore constant at a fixed point relative to the upper plane. The distance between the planes is given by:

$$e(x) = e_1 + \theta x,$$

where the angle $\theta = (e_2 - e_1)/L$ is assumed to be small. In this case, and if $Re \ll 1/\theta$, Equation 8.11b shows that the pressure p and, therefore, $\partial p/\partial x$ are independent of y.

Integrating Equation 8.11a with respect to y under this assumption and taking into account the boundary conditions $v_x(y=0) = -U$ and $v_x(y=e(x)) = 0$, we obtain then:

$$v_x(x, y) = -\frac{1}{2\eta}\frac{dp}{dx}\, y\,[e(x) - y] - U\,\frac{e(x) - y}{e(x)}. \tag{8.12}$$

Just as in Section 4.5.3, the velocity field corresponds to the superposition of a Poiseuille flow (parabolic term in y associated with the pressure gradient) and of a Couette flow (term linear in y, related to the movement of the plane with velocity $-\mathbf{U}$). In Figure 8.2a, we have shown the parabolic velocity profiles between the two planes corresponding to different distances along x.

We compute now the pressure distribution in the upper plane by integrating Equation 8.12 with respect to y between 0 and $e(x)$; the flow rate Q (per unit depth in the z-direction) is constant with x because the flow is stationary in the reference frame selected so that:

$$Q = \text{constant} = \int_0^{e(x)} v_x \mathrm{d}y = -\frac{1}{\eta}\,\frac{\mathrm{d}p}{\mathrm{d}x}\,\frac{e(x)^3}{12} - \frac{U\,e(x)}{2}. \tag{8.13}$$

As we might have expected, this equation coincides with Equation 4.72 when we replace V_0 by $-U$ and a by $e(x)$. We therefore conclude, replacing x by e as the variable:

$$\frac{\mathrm{d}p}{\mathrm{d}x} = \theta\,\frac{\mathrm{d}p}{\mathrm{d}e} = -\frac{12\,\eta\,Q}{e(x)^3} - \frac{6\,\eta U}{e(x)^2}. \tag{8.14}$$

We can obtain the value e_m of the thickness at the point where the pressure has an extreme value ($\mathrm{d}p/\mathrm{d}e = 0$), so that:

$$e_m = -2\,\frac{Q}{U}. \tag{8.15}$$

Finally we obtain the pressure $p(x)$ by integrating Equations 8.14 relative to e with $p\,(x = 0) = p_0$ (atmospheric pressure outside the thin film). We find that:

$$p(x) = p_0 + \frac{6\,\eta\,Q}{\theta}\left[\frac{1}{e(x)^2} - \frac{1}{e_1^2}\right] + \frac{6\,\eta U}{\theta}\left[\frac{1}{e(x)} - \frac{1}{e_1}\right]. \tag{8.16}$$

From this, we determine the value of the flow rate Q by writing that the pressure is also equal to p_0 at the other end of the plane (where $e = e_2$). We then obtain:

$$Q = -\frac{e_1\,e_2}{e_1 + e_2}U; \qquad (8.17) \qquad \text{whence:} \qquad e_m = 2\,\frac{e_1\,e_2}{e_1 + e_2}. \tag{8.18}$$

Equation 8.18 indicates that, when $e_1 \ll e_2$, we have $e_m \cong 2e_1$: the point where the pressure has an extreme value is then very close to the side where the thickness has the value e_1. In all cases, according to Equation 8.17, Q and U are opposite in sign, i.e. the average flow of the fluid has the direction of the motion of the lower plane. Equations 8.16 can then be transformed by replacing Q by its value as a function of U, so that we obtain:

$$p(x) = p_0 + \frac{6\,\eta U}{\theta}\,\frac{(e_2 - e(x))\;(e(x) - e_1)}{e(x)^2\;\;(e_1 + e_2)}. \tag{8.19}$$

The difference $p\,(x) - p_0$ has then necessarily the same sign as U/θ, since $e(x)$ is bounded by the values e_1 and e_2. Figure 8.2b gives the corresponding pressure distribution.

The normal force F_N on the lower plane, due to this excess pressure resulting from the flow, is given by the integral:

$$F_N = -\int_0^L (p - p_0)\,\mathrm{d}x = -\frac{1}{\theta}\int_{e_1}^{e_2} (p - p_0)\,\mathrm{d}e = -\frac{6\,\eta U}{\theta^2}\left[\mathrm{Log}\,\frac{e_2}{e_1} - \frac{2\,(e_2 - e_1)}{e_2 + e_1}\right]. \tag{8.20}$$

Let us consider the velocity profiles between the two planes on the basis of Equations 8.12, taking the derivative with respect to y and replacing $\partial p/\partial x$ by $\theta(\partial p/\partial e)$, and $\partial p/\partial e$ by combining Equations 8.14 and Equations 8.17. We are specifically interested in the existence of a maximum in the velocity profile. We take the derivative:

$$\frac{\partial v_x}{\partial y} = \frac{2y - e(x)}{2\eta}\theta\frac{\partial p}{\partial e(x)} + \frac{U}{e(x)} = \frac{2U}{e(x)^2}\left[\frac{3e_1e_2\,(2y - e(x))}{e(x)(e_1 + e_2)} + 2e(x) - 3y\right]. \tag{8.21}$$

Near the lower wall ($y = 0$) and the upper wall ($y = e(x)$), we have, respectively:

$$\frac{\partial v_x}{\partial y} = \frac{2\,U}{e(x)^2}\left[-\frac{3\,e_1\,e_2}{(e_1 + e_2)} + 2\,e(x)\right] \tag{8.22a}$$

and

$$\frac{\partial v_x}{\partial y} = \frac{2\,U}{e(x)^2}\left[\frac{3\,e_1\,e_2}{(e_1 + e_2)} - e(x)\right]. \tag{8.22b}$$

The derivatives $\partial v_x/\partial y$ of the velocity profile on the upper and lower planes then vanish, respectively when $e\,(x_1) = 3e_1e_2/\,(2\,(e_1 + e_2)) = 3e_m/4$ and $e\,(x_2) = 3e_1e/\,(e_1 + e_2) = 3e_m/2$, i.e. on both sides of the point where the pressure is a maximum. For distances smaller than x_1, the velocity has a minimum; for distances greater than x_2, the velocity is positive in the neighborhood of the upper wall, and it has a maximum. In the section of thickness e_m corresponding to the pressure maximum, the velocity varies linearly with the distance y: this is easily shown by taking the second derivative $\partial^2 v_x/\partial y^2$ of the velocity profile $v_x(y)$ from Equation 8.21 so as to obtain $\partial^2 v_x/\partial y^2 = (\theta/\eta)(\partial p/\partial e(x))$. The distance x at which the curvature becomes zero corresponds to the maximum in the pressure: this is quite expected since, in the absence of a pressure gradient, the Poiseuille component of the flow becomes zero and only a Couette-type flow remains.

We also determine the tangential frictional force on the lower plane, i.e.:

$$F_T = \int_0^L \eta \frac{\partial v_x}{\partial y} \mathrm{d}x = \frac{1}{\theta} \int_{e_1}^{e_2} \left(\frac{e(x)}{2} \frac{\mathrm{d}p}{\mathrm{d}x} + \frac{\eta U}{e(x)} \right) \mathrm{d}e = \frac{2\eta U}{\theta} \left[2 \operatorname{Log} \frac{e_2}{e_1} - \frac{3(e_2 - e_1)}{(e_2 + e_1)} \right]. \tag{8.23}$$

The net resultant force on the fluid in the space between the planes must be zero since the pressure difference between the entry and exit of this space is also zero. The x- and y-components of the force on the upper plane must therefore be equal to $-F_T$ and $-F_N$; they can also be computed from the pressure and velocity on that plane. However, the pressure and tangential forces are respectively perpendicular and parallel to the plane and, therefore, at an angle θ respectively to y and x: they must then be projected on these axis in order to retrieve the values $-F_T$ and $-F_N$.

For $e_2/e_1 = 10$, the prefactors of $\eta U/\theta^2$ and $\eta U/\theta$ respectively in Equations 8.20 and 8.23 are –4 and 4.3.

In the general case, the relative role of the values of θ, e_1 and e_2 is somewhat subtle because, when $\theta \to 0$ and $e_2 \to e_1$, both the numerator and the denominator of the expressions for F_T and F_N approach zero. We will evaluate these two components for the particular case where the thickness e_2 is much greater than the thickness e_1. In that case, we find:

$$F_N \simeq -\left(\operatorname{Log} \frac{e_2}{e_1} - 2 \right) \frac{6\eta U}{\theta^2} \qquad \text{(8.24a)} \qquad \text{and} \qquad F_T \simeq \left(4 \operatorname{Log} \frac{e_2}{e_1} - 6 \right) \frac{\eta U}{\theta}. \qquad \text{(8.24b)}$$

From Equations 8.24a–b, F_T and F_N are approximately proportional to $1/\theta$ and $1/\theta^2$ only, provided $e_2/e_1 \gg 1$ (then, $\theta \approx e_2/L$). If $e_2/e_1 \to 1$, we must use Equations 8.20 and 8.23, leading to $F_N = 0$ when $e_2 = e_1$ (parallel planes).

where $\theta = (e_2 - e_1)/L \simeq e_2/L$ (for a given angle θ, the influence of e_2/e_1 on the values of F_T and F_N is small). When the angle θ is small, F_N can take on large values, while the tangential frictional force F_T will be smaller by an order of magnitude: this is the fundamental result of the lubrication model.

This property is extremely useful in a wide range of applications: axles rotating within a bearing of barely larger diameter, thus able to support much greater normal stresses without excessive friction (*bearings* of rotating machinery, *wheel axles* of vehicles. . .). In some cases, the normal forces are so large that solid pieces can be deformed in regions where their cross-section is very small; for this reason they are known as *elasto-hydrodynamic forces*.

Lubrication forces can also have rather undesirable effects: if we walk on an oil slick, the normal forces will support our weight while the tangential force is insufficient to allow us to maintain our balance. There is a similar effect when a car skids out of control along a wet road (a phenomenon known as *aquaplaning*): the thin film of water between the tires and the road can support the weight of a car, while the forces that prevent slip are too weak.

For $e_2 \gg e_1$, $p(x)$ is highest for $e(x) \approx 2e_1$. More generally, in lubrication flows, the pressure is highest in the regions of small liquid thickness: this allows one to obtain approximate solutions. Take, for instance, two spheres of radius R approaching each other with a minimum separation $e_1(t)$: the force between them may be estimated from the pressure distribution on the spherical cap with radius $\sqrt{R e_1(t)}$ where the local separation between the surfaces of the two spheres is between e_1 and $2e_1$ (see similar problems below).

8.1.6 Flow of a fluid film of arbitrary thickness

In this section, we consider the more general case of a flow of a thin film of fluid between two solid surfaces with varying separation, and with relative motion in arbitrary directions.

Reynolds' equation

We retain the assumption of a film of fluid sufficiently thin relative to the characteristic distances along x over which the velocity and the thickness parallel to the film vary, so that we can still consider the flow as quasi-parallel (Figure 8.3). We also assume that the lower surface is a stationary plane $y = 0$ and that each point of the upper surface located at a height $h(x, t)$ has a velocity with components $U(x, t)$ and $V(x, t)$ in the x- and y-directions. The longitudinal pressure gradient $\partial p/\partial x$ is considered constant over the thickness of the film, but can exhibit a slow variation along this film. As seen in Section 8.1.2, the term $\partial p/\partial x$ needs to be replaced by $\partial p/\partial x - \rho\, g_x$ when the component g_x of gravity in the plane of the film does not vanish. In the present section, the upper surface is solid but not necessarily plane.

As in the preceding case, the local flow is a superposition of a Poiseuille-type and a Couette-type flow. This can result from the relative displacement of the solid walls, which limits the upper and lower surfaces of the film and/or, possibly, by an applied pressure gradient.

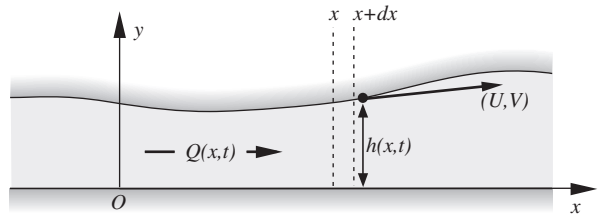

Figure 8.3 *Schematic diagram of a quasi-one-dimensional flow in a thin fluid layer between a plane and a solid upper surface with a distance h(x, t) from the plane, which can be a function of both time and position*

Let us rewrite Equations 8.13 relating the local flow rate $Q(x, t)$ in the film (per unit length in the z-direction), the gradient $\partial p/\partial x$ and the velocity component $U(x, t)$ in the x-direction of the upper surface, with:

$$Q(x,\ t) = -\frac{h^3}{12\ \eta}\ \frac{\partial p}{\partial x} + \frac{U\ h}{2}. \tag{8.25}$$

In contrast with the case of Equations 8.13, Q can depend on x as well as on t. Let us now analyze the conservation of mass in a thin layer of the fluid film over the range $(x,\ x + \mathrm{d}x)$: the change $(\partial h/\partial t)\mathrm{d}x$ of the volume of fluid in this layer, per unit time, is equal to the difference $Q(x) - Q(x + \mathrm{d}x) = -(\partial Q/\partial x)\mathrm{d}x$ between the rates of flow of fluid entering and exiting. We thus obtain, by taking the derivative of Equations 8.25 with respect to x:

$$\frac{\partial h}{\partial t} = \frac{1}{12\ \eta}\ \frac{\partial}{\partial x}\left[h^3\ \frac{\partial p}{\partial x}\right] - \frac{1}{2}\left(h\ \frac{\partial U}{\partial x} + U\ \frac{\partial h}{\partial x}\right). \tag{8.26}$$

This result applies to a two-dimensional flow, translationally invariant in the z-direction. Equation 8.26 is known as *Reynolds' equation*. In practice, we frequently fix the values of the pressure at the two ends of the fluid layer.

Let us now take note of the fact that the vertical V and horizontal U components of the local velocity of the wall are related to the derivative $\partial h/\partial t$ by the geometric condition:

$$\frac{\partial h}{\partial t} = V - U\ \frac{\partial h}{\partial x}. \tag{8.27}$$

A horizontal displacement of the upper wall results indeed in a change in the local depth, if the wall itself is not locally horizontal. This variation is added to that resulting from the vertical velocity V of the wall. We see then, according to Equations 8.27, that h remains constant if the upper wall moves in its own plane ($V/U = \partial h/\partial x$).

In the case of a two-dimensional film, where the thickness $h(x, z, t)$ varies in the x- and z-directions parallel to the lower plane, we must replace Equations 8.25 by:

$$\mathbf{Q}_{//}(x,\ z,\ t) = -\frac{h^3}{12\ \eta}\ \nabla_{//}\, p + \frac{\mathbf{U}_{//}\ h}{2}, \tag{8.28}$$

where $\mathbf{U}_{//}$ is the projection onto the z-x plane of the velocity $\mathbf{U}$ of the upper surface with respective components W and U in the z- and x-directions. The components Q_z and Q_x of $\mathbf{Q}_{//}$ represent the local rates of flow through unit cross-sections respectively perpendicular to the z- and x-directions. The symbol $\nabla_{//}$ indicates the gradient in the directions parallel to the plane. By writing the equation of conservation of mass in the three-dimensional form $\partial h/\partial t + \nabla\cdot\mathbf{Q}_{//} = 0$, we obtain the generalization of Equations 8.26:

$$\nabla\cdot\left[h^3\ \nabla_{//}p\right] = h^3\ \nabla^2 p + 3\ h^2\ (\nabla_{//}h)\cdot(\nabla_{//}p) = 6\eta\left(h\ \nabla_{//}\cdot\mathbf{U}_{//} + \mathbf{U}_{//}\cdot(\nabla_{//}h) + 2\frac{\partial h}{\partial t}\right). \tag{8.29}$$

The problem in Section 8.1.5 (flow between two planes at an angle θ) can be treated as a particular case of Reynolds' equation (Equation 8.26) with $\partial h/\partial t = -U\ \partial h/\partial x$, $h(x) = e(x)$ and $\partial e/\partial t = -U\ \partial e/\partial x$. In this former section, we used a reference frame fixed relative to the upper plane, where the flow was stationary, whereas, here, we are in a reference frame fixed with respect to the lower plane and in which ∂h/∂t is non-zero (the local velocity of the upper plane is then $+U$). Equations 8.26 then becomes:

$$\frac{\partial}{\partial x}\left[h^3\ \frac{\partial p}{\partial x}\right] = -6\ \eta U\ \frac{\partial h}{\partial x}. \tag{8.31}$$

We obtain the same equation by multiplying Equations 8.14 by $e(x)^3$ and taking the derivative with respect to x (Q is constant relative to x in the reference frame used in Section 8.1.5, while, here, it varies).

Similarly, Equations 8.27 becomes:

$$\frac{\partial h}{\partial t} = V - \mathbf{U}_{//} \cdot \boldsymbol{\nabla}_{//} h. \tag{8.30}$$

Application of Reynolds' equation: a sphere dropping toward a plane, in a viscous fluid

Consider a rigid sphere of radius a dropping vertically toward an horizontal flat plane (Figure 8.4): we denote by $h_0(t)$ the minimum distance between the sphere and the plane, i.e. along the axis of the system. Considering the rotational symmetry (the pressure being solely a function of r and t) and the condition $\mathbf{U}_{//} = 0$, Equations 8.29 becomes:

$$\frac{1}{r}\frac{\partial}{\partial r}\left[r\, h^3 \frac{\partial p}{\partial r}\right] = 12\eta\, \frac{\partial h}{\partial t} \qquad (8.32) \qquad \text{with} \qquad \frac{\partial h}{\partial t} = \frac{\mathrm{d}h_0(t)}{\mathrm{d}t}.$$

This last condition corresponds to the requirement of a uniform vertical velocity $\partial h/\partial t$ for all points of the surface of the sphere. We can calculate the global force $\mathbf{F}$ on the sphere by integrating the pressure:

$$F = \int_0^{r_M} 2\pi\, r\, p(r)\, \mathrm{d}r = \int_{h_0}^{h_M} 2\pi a\, p(h)\, \mathrm{d}h,$$

so that we obtain:

$$F = -\frac{6\,\pi\, a^2}{h_0}\frac{dh_0}{dt}, \tag{8.33}$$

provided that the thickness h_M as we get away from the region of minimum depth is significantly greater than h_0.

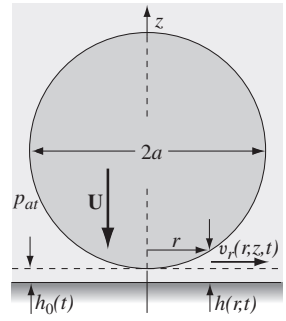

Figure 8.4 *Schematic diagram for a sphere dropping toward an infinite plane*

Proof

In order to calculate $p(h)$, we first integrate Equations 8.32 with respect to r, after having multiplied both sides by r. We then obtain:

$$r\, h^3 \frac{\partial p}{\partial r} = 6\,\eta\, r^2 \frac{\partial h}{\partial t}. \tag{8.34}$$

The constant of integration is zero because none of the derivatives diverge when $r = 0$. In order to calculate the pressure distribution, we substitute h for the variable r, by using the approximate geometrical relationship:

$$h(r,\ t) = h_0(t) + \frac{r^2}{2a}, \tag{8.35}$$

whence $\mathrm{d}h = r\,\mathrm{d}r/a$ and $\mathrm{d}p/\mathrm{d}r = (r/a)\,\mathrm{d}p/\mathrm{d}h$.

Thus: $$\mathrm{d}p = -3\,\eta\, a \frac{\mathrm{d}h_0}{\mathrm{d}t}\mathrm{d}\left[\frac{1}{h^2}\right] \qquad \text{and} \qquad p(h) = p_0 - \frac{3\,\eta\, a}{h^2}\frac{\mathrm{d}h_0}{\mathrm{d}t}. \tag{8.36}$$

The pressure must indeed be equal to the atmospheric pressure p_0 when h becomes large.

For a sphere of radius a, falling under its own weight and with respective densities ρ_s and ρ_f of the sphere and the fluid, we find, by equating the weight of the sphere, decreased by the buoyancy due to the Archimedes force, to the viscous force from Equations 8.33 that:

$$\frac{\mathrm{d}(\mathrm{Log}\, h_0)}{dt} = -\frac{2\pi}{9}\,\frac{a\,(\rho_s - \rho_f)g}{\eta} \qquad (8.37) \qquad \text{i.e.:} \qquad h_0(t) = h_0(0)\ \mathrm{e}^{-t/\tau}, \qquad (8.38)$$

with $\tau = 9\,\eta/[2\pi a\ (\rho_s - \rho_f)\ g]$. Theoretically, the sphere will take an infinitely long time to touch the plane because its motion is continuously slowing down! Practically, however, the roughness of the surfaces involved will lead to contact when the separation becomes of the order of this micro-roughness, although there still remains a tiny free space for the fluid to be evacuated.

For the case where the sphere is replaced by a flat-bottomed cylinder parallel to the plane, we find that the force varies as $1/h^3$ instead of $1/h$ for a given velocity, because the viscous forces are more uniformly distributed over the bottom of the cylinder, instead of being localized in the region of minimum thickness.

If, on the other hand, we specify a drop velocity $V_z = \mathrm{d}h/\mathrm{d}t$, the force that needs to be applied for keeping V_z constant diverges, according to Equations 8.36, as $1/h_0$ when the distance h_0 approaches zero, while the pressure diverges as $1/h_0^2$ in the region of minimum thickness h_0: this can result in a local deformation of the surface of the sphere.

8.1.7 Flow between two eccentric cylinders with nearly equal radii

An important industrial application of lubrication is the motion of moving objects with a narrow region between the parts (piston-and-cylinder, axle-and-bearing, etc.) filled with lubricating fluid.

Here we are specifically interested in the flow of the lubricant in the small gap between a rotating axle and its bearing, as well as in the forces which result from it: this system is schematized in Figure 8.5 by two cylinders of nearly equal radii R and $R + \delta R$ ($\delta R/R = \varepsilon \ll 1$), with their axes parallel but offset by a distance $a = \lambda\,\delta R$ ($\lambda \leq 1$). We assume that only the inner cylinder rotates at an angular velocity Ω and that the flow is invariant in the z-direction of the axes of the cylinders. We will take, as the origin of the polar coordinates, the point of intersection O of the axis of the larger cylinder with the plane of the figure; the angle $\theta = 0$ corresponds to the direction of the segment **OO'** (and, also, to the minimum e_0 of the local distance $e(\theta)$ between the cylinders); α is the angle that **OO'** makes with the vertical. The distance $e(\theta)$ satisfies the equation:

$$e\,(\theta) = \delta R - a\cos\theta = \varepsilon R\,(1 - \lambda\cos\theta). \qquad (8.39)$$

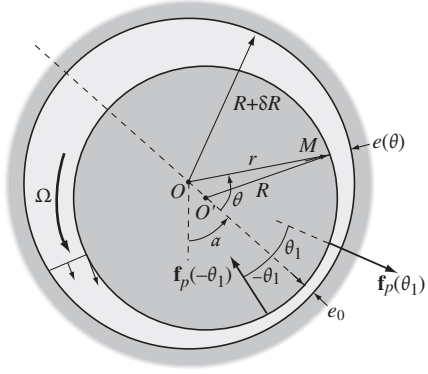

Figure 8.5 *Schematic diagram of the cross-section of an axle rotating within its bearing, the z-axis being perpendicular to the plane of the figure. The points O and O′ correspond to the intersection of the axes of the two cylinders with the plane of the figure*

Proof

The distance $r = |\mathbf{OM}|$ between O and a point M of the inner cylinder such that $\mathbf{OM}$ makes an angle θ with the segment $\mathbf{OO}'$ connecting the axes satisfies, to first-order:

$$r = R + a\cos\theta = R + \lambda\,\delta R\,\cos\theta$$

Equation 8.39 is then obtained by subtracting r from the radius $R+\delta R$ of the outer cylinder and replacing δR *by* εR.

In the region around a given angle θ, we consider that the flow is identical to that between two parallel planes separated by a distance $e(\theta)$, one of which (corresponding to the inner cylinder) moving at a velocity ΩR. This assumption is equivalent to eliminating curvature effects, such as the gradient in the pressure due to the centrifugal force; the latter is actually transverse to the flow and does not affect it. We can then apply Reynolds' equation (Equations 8.26) in the form:

$$\frac{1}{R^2}\frac{\partial}{\partial\theta}\left[e(\theta)^3\frac{\partial p}{\partial\theta}\right] = 6\,\eta\,\Omega\frac{\partial e(\theta)}{\partial\theta} \quad (8.40) \qquad \text{so:} \qquad \frac{\partial p}{\partial\theta} = 6\,\eta\,\Omega\,R^2\frac{1}{e(\theta)^2} + \frac{C}{e(\theta)^3}, \quad (8.41)$$

where C is a constant of integration. In order to go from Equations 8.26 to Equations 8.41, we have merely replaced the derivatives $\partial/\partial x$ by $(1/R)\,\partial/\partial\theta$. The element of length $\mathrm{d}s$ in the direction tangent to the surfaces of the cylinders, corresponding to an angular change $\mathrm{d}\theta$, is indeed equal to $R\,\mathrm{d}\theta$ (still assuming that $\delta R \ll R$); $\mathrm{d}s$ here plays the role of $\mathrm{d}x$ in the problem involving planes. Figure 8.6 displays the changes in pressure as a function of θ calculated for $\lambda = 0.9$, by numerical integration of Equations 8.41, and using Equations 8.39. We have large minima and maxima of the pressure near $x = 0$ because of the large value of the term in $1/e^3$: we can observe here cavitation bubbles in the region of low pressure (see Section 8.3.2).

The characteristics of the curve in Figure 8.6 result from the form of Equations 8.38 and 8.41. The variation of $e(\theta)$ and that of $\partial p/\partial\theta$ are symmetric with respect to $\theta = 0$: as a result, the pressure changes $p(\theta) - p(0)$ obtained by integration are anti-symmetric. We must, moreover, also have the condition that $p(\pi) = p(-\pi)$ since these two values of θ correspond to the same physical location diametrically opposite to the point of minimum thickness. If $p(\theta)$-$p(0)$ is not constant, it must have, at least, two extrema of opposite signs at points which are symmetric relative to $\theta = 0$ so that the constant C must be opposite in sign to Ω (see Equations 8.41). In the neighborhood of $\theta = 0$, the term $1/e^3$ in Equations 8.41 dominates the other term, and the derivative $\partial p/\partial\theta(0)$ is opposite in sign to Ω (< 0 in Figure 8.6). The presence of the term in $1/e^3$ implies that the smaller the minimum thickness $e(0)$ is relative to the maximum value $e(\pi)$, the larger the absolute values of the pressure extrema will be, and closer to the point $\theta = 0$.

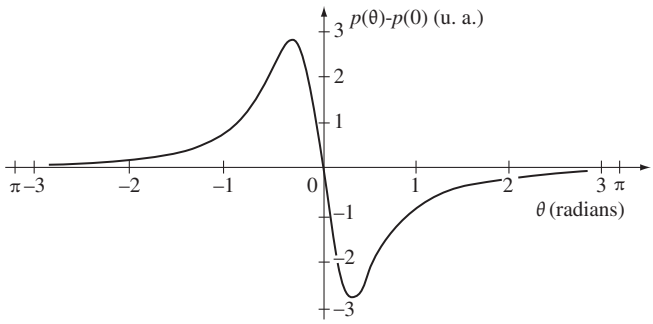

Figure 8.6 *The variation of the pressure in the region between the axle and its bearing in Figure 8.5*

Just as in the case of the two planes which we discussed in Section 8.1.5, we assume that the viscous friction forces, which act tangentially to the cylinders, are negligible relative to the pressure forces in the normal direction. Let us now investigate how these forces can support heavy weights as in the cases of a wheel axle or of the axis of rotating machinery. To this end, let us look at the pressure forces per unit area $\mathbf{f}_p = \mathrm{d}\mathbf{F}_p/\mathrm{d}S$ acting on the inner cylinder at corresponding points θ_1 and $-\theta_1$ (Figure 8.5). We can neglect the effect of the

The form of equation 8.43 may seem counter-intuitive. We might think that the force of gravity would require the point of minimal thickness to be at the lowest point of the bearing in the vertical direction from the axis O: **OO'** would be in that case vertical with $\alpha = 0$. However, the vertical resultant of the pressure forces would vanish, because the contribution of each point at a position θ is cancelled out by that of a point at the angle $-\theta$: the pressure $p(\theta)$ is then opposite to that at $p(-\theta)$ and the vertical component of the normal to the surface is the same. In contrast, if $\alpha = \pi/2$, the pressure force also changes sign when we replace θ by $-\theta$, but so does the vertical component of the normal to the surface. The contributions to the force then have the same sign and they add up. The value of α will adjust to a value intermediate between 0 and $\pi/2$ depending on the weight which must be supported.

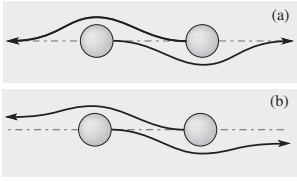

Figure 8.7 *Relative motion of two spheres. (a) ideal case without any interaction other than those due to hydrodynamics; (b) Real case of rough spheres: the two spheres undergo a shift in their trajectories, instead of coming back on the same straight line which they followed initially (an analogous effect is observed in the case where the two spheres display inter-particle interactions such as electrostatic repulsion)*

The reversibility argument assumes that the velocity field takes on, at every instant, the equilibrium configuration which corresponds to the instantaneous distance between the obstacles; we have described a similar problem in Section 8.1.3 which discussed the stationarity of lubrication flows. When the two spheres come together at a distance d, with relative velocity U, the time for establishing the velocity profile is of the order of d^2/ν: this must be small relative to the characteristic time d/U over which the distance between particles evolves. The Reynolds number Ud/ν must then be small. In the opposite case, the dynamics of the motion of the sphere would depend on its previous history. We encounter effects of this type, for which we will not go into detail here, in the case of strongly accelerating particles (specifically, effects known as *Basset forces*).

average pressure $p(0)$ because the integral of the force which results on the entirety of each cylinder is zero. We will therefore assume that $p(\theta_1) = -p(-\theta_1)$. The sum of the vertical components $f_{zp}(\pm\theta_1)$ of the pressure forces per unit area at θ_1 and $-\theta_1$ will be:

$$f_{zp}(\theta_1) + f_{zp}(-\theta_1) = -p(\theta_1)\cos(\alpha+\theta_1) + p(-\theta_1)\cos(\alpha-\theta_1) = 2p(\theta_1)\sin\alpha\sin\theta_1. \quad (8.42)$$

Thus, the vertical resultant of the pressure forces is a maximum when the angle α of **OO'** with the vertical has the value $\pi/2$ (**OO'** is then horizontal). The value $F_{p\pi/2}$ of this force per unit length along the axis is then given by the integral:

$$F_{p\pi/2} = -\int_{-\theta}^{\theta} \sin(\theta)\, p(\theta) R\, d\theta \text{ which can be shown to equal to: } F_{p\pi/2} = \frac{6\,\eta A\,\Omega\,R}{\varepsilon^2\,\lambda}. \quad (8.43)$$

Here, A is a constant dependent on λ. This bearing force varies as $1/\varepsilon^2$: when ε is very small, one can generate very significant bearing forces.

Let us now evaluate the viscous frictional force $F_{v\,\pi/2}$ in the direction of $\theta = \pi/2$. Per unit area, this force is of the order of $\eta\,\Omega\;R/((1-\lambda)\,\varepsilon\,R)$ in the region of minimum thickness; if this is applied along a distance of order R, we obtain then:

$$F_{v\pi/2} \approx \frac{\eta\,\Omega\,R}{(1-\lambda)\,\varepsilon}. \quad (8.44)$$

This viscous frictional force, varying as $1/\varepsilon$, is smaller than the bearing force by an order of magnitude in ε, as we have assumed.

8.1.8 Lubrication and surface roughness

The examples which we have given and, specifically, that of the axle and its bearing, suggest that the distance between the solid surfaces should be as small as possible: this will be limited by the roughness of the surfaces which, in our calculations, have been assumed to be perfectly smooth. If the rough areas of the surfaces actually come into contact, there will appear solid-solid frictional forces which would block any motion. Another example is the interaction between particles in a suspension when they are separated by a small distance. As we have seen in Section 8.1.5, the viscous forces increase when a sphere approaches a wall very closely; when the distance becomes small, we must again take into account the effects of surface roughness. An example is given in Figure 8.7. In the case of two perfectly smooth spheres which come together, the final trajectory coincides with the line of initial displacement (Figure 8.7a): this is the result of the time-reversal invariance in solutions of Stokes' equation of motion at small Reynolds number (see Section 9.2.3). This reversibility can be broken by the effect of the roughness of the particles (Figure 8.7b). Quite a number of problems related to lubrication, to friction and to wear depend on the heterogeneity of surfaces.

8.2 Flow of liquid films having a free surface: hydrodynamics of wetting

Other situations where inertial forces and non-linear terms in the equations of motion of fluids are negligible are encountered in the case of thin fluid films with a free surface: there again, the velocity of the fluid is almost parallel to the surface of the film. Such flows are often present in nature and have, additionally, important applications such as the spreading

of coatings, paints or cleaning fluids on various materials; also, some thermal exchangers make use of flowing liquid films. This situation is similar to that of lubrication, but the presence of free surfaces affects the boundary conditions, and additional forces appear due to surface tension. We have discussed this idea in Section 1.4 and have described some static properties of the resulting interfaces. Using the Young-Dupré equation (Equation 1.62), we have also introduced the spreading parameter and the static contact angle.

In this discussion, we are interested in flows of thin films with a free surface resulting from a competition between surface tension, gravity and viscosity. In all cases, we will make broad use of the lubrication approximation.

First of all, we analyze the simple case of the flow of liquid layers uninfluenced by surface tension, such as the falling of a liquid film along a flat isothermal wall. Then, in the situation of complete wetting, we study the dependence of the dynamic contact angle of an interface on the velocity at which the contact line moves. We use this result to predict the spreading of small droplets and compare this to that of larger drops under the influence of gravity. Finally, we look at the case of *Marangoni effects* in which temperature or concentration gradients, in tensioactive compounds, result in surface tension gradients, which, themselves, induce flow.

8.2.1 Dynamics of thin liquid films, neglecting surface-tension effects

The influence of surface tension is negligible for films which have a surface flat or slightly curved because the difference in the Laplace pressure between the two sides of the interface is then either zero or very small. We will discuss situations where the surface tension is constant all over the surface so that Marangoni effects will not come into play.

Flows of liquid films with a free surface have specific characteristics. First of all, if surface tension is not in play, the pressure equals the atmospheric pressure throughout the interface. Just as for other quasi-parallel flows, the pressure gradients normal to the interface (and thus normal to the flow velocity) are reduced to the hydrostatic pressure. Given the small thickness of the films, the pressure is everywhere close to the atmospheric pressure: the pressure gradients parallel to the film (and to the velocity of the fluid) are thus generally much smaller than for the flows between two solid surfaces which we have previously considered. Often, this gradient will be zero (specifically for films of constant thickness) and the driving force of the flow is the component $g_{//}$ of gravity parallel to the surface of the film: we recall that in the Stokes equation (and in that of Navier-Stokes), the driving force of the flow is represented by the sum $\nabla p - \rho\,\mathbf{g}$ and not just by ∇p.

If, externally, we have air at rest (or at moderate velocities), we can consider that the stress at the interface vanishes (Section 4.3.2): the derivative of the velocity in the direction normal to the surface thus also vanishes. We have then an extremum of the velocity at the surface and not a zero value as would be the case at a solid wall.

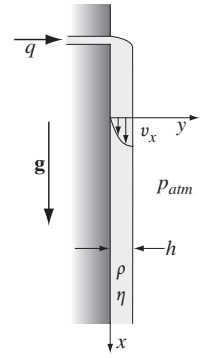

Figure 8.8 *Flow along a vertical wall due to an injection of fluid through a horizontal slit*

This will no longer be the case when there is a high-velocity flow of air (e.g., high winds above the surface of a lake or river.)

Example: viscous film falling along a vertical wall, at a fixed flow rate

We can create a fluid film (density ρ, viscosity η) along a vertical wall by injecting fluid through a horizontal slit (Figure 8.8). The flow rate q in the slit, per unit width in the z-direction, is constant. We shall now predict the dependence of the thickness of the fluid layer on the flow rate q, in the region where this layer has a constant thickness h. Assuming that the flow is invariant and has zero velocity in the z-direction, the Navier-Stokes equations become:

$$\frac{1}{\rho}\frac{\partial p}{\partial x} - \rho g = \eta\frac{\partial^2 v_x}{\partial y^2} \qquad (8.45a) \qquad \text{and} \qquad \frac{\partial p}{\partial y} = 0. \qquad (8.45b)$$

For sufficiently large velocities, such flows develop instabilities which cause the thickness of the film to vary and create local curvature at the surface. Then, one needs to take into account both the surface tension and the pressure gradients parallel to the surface.

We obtain similar results for a flow along a plane inclined at an angle θ relative to the vertical. We must then replace $-\rho\ g$ by $-\rho\ g\cos\theta$ in Equations 8.45a and add a term $-\rho g\sin\theta$ into Equation 8.45b. However, since this last term is constant, $\partial p/\partial x$ still vanishes even though the hydrostatic pressure gradient in the y-direction no longer vanishes. Equations 8.46a and 8.46b remain applicable when we replace g by $g\cos\theta$.

Because we have constant external pressure, continuous at the surface and continuous at all horizontal levels, we have $p = p_{atm}$ throughout the fluid film: the pressure gradient parallel to the velocity also vanishes ($\partial p/\partial x = 0$). The flow thus results merely from the vertical component $g > 0$ of gravity. Integrating with the boundary conditions, $v_x(y=0) = 0$ and $\partial v_x/\partial y(y = h) = 0$, we find:

$$v_x = \frac{\rho\ g}{2\ \eta} y\ (2\ h - y) \qquad (8.46a) \qquad \text{and} \qquad q = \int_0^h v_x\ \mathrm{d}y = \frac{\rho\ g\ h^3}{3\ \eta}. \qquad (8.46b)$$

The thickness of the fluid layer varies with the injected rate of flow as $q^{1/3}$.

8.2.2 Dynamic contact angles

Case of complete wetting: Tanner's law

In contrast to the previous example, surface tension plays a key role in problems involving the contact line between a gas-liquid interface (or a liquid-liquid interface) and a solid surface. Here, we are interested in the changes, of hydrodynamic origin, in the contact angle as a function of the velocity V of the line: it is referred to as a *dynamic contact angle*. We consider here the case of complete wetting for which the initial spreading parameter $S = \gamma_{sg} - \gamma_{sl} - \gamma$ (defined in Equation 1.59) is positive (we use here the notation γ for γ_{lg}). The motion of the interface at a velocity V changes the contact angle from the value $\theta_s = 0$ (*static contact angle*) for $V = 0$ to a finite value $\theta(V)$. In such systems with complete wetting, we always have, upstream of the contact line, a precursor film of submicron thickness: the dynamic contact angle $\theta(V)$ is in fact an *apparent contact angle*, with the wall, of the *macroscopic* region of the meniscus (Figure 8.9).

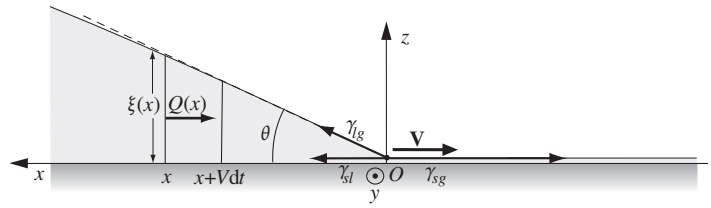

Figure 8.9 *Schematic diagram for the motion of a contact line relative to a solid surface in the presence of the precursor film upstream of the meniscus*

Let us first consider the equilibrium of forces acting on the contact line by assuming a two-dimensional geometry. Following the same steps as those used in Chapter 1 in order to prove the Young-Dupré equation (Equation 1.62), we find a resultant force, per unit length, with horizontal component: $F_r(\theta\ ) = \gamma_{sg} - \gamma_{sl} - \gamma\cos\theta$. However, according to this equation, the condition of static equilibrium $F_r = 0$ cannot be satisfied at zero velocity even when $\theta = 0$. The excess force per unit length equals $S(> 0)$, and we assume that its use is to create the precursor film, and that this contribution remains constant when V is not zero. The effective resultant force which causes the motion of the region of macroscopic thickness of the meniscus (to the left of the point O on Figure 8.9) is thus: $F_r(\theta) - S = \gamma(1 - \cos\theta)$. The corresponding power (energy per unit time) $\mathrm{d}E_{ts}/\mathrm{d}t$ is then:

$$\frac{\mathrm{d}E_{ts}}{\mathrm{d}t} = \gamma\ (1 - \cos\ \theta)\ V. \qquad (8.47)$$

This energy, provided by the capillary forces, is dissipated through viscosity in the flow of the film resulting from the motion of the interface. We note that $\mathrm{d}E_{ts}/\mathrm{d}t$ should vanish for

an angle $\theta = 0$, which would correspond to an almost motionless interface for which all the available energy is dissipated in the residual film.

Let us now analyze the flow in the macroscopic region of the fluid film of thickness $\xi(x)$ at a distance x from the contact line. We assume that we are sufficiently close to this contact line that gravity effects are negligible for the small vertical distances which we are considering. We will also assume that the apparent macroscopic contact angle θ is sufficiently small that we can use everywhere the lubrication approximation. Let us call $Q(x)$ the rate of flow (per unit length normal to the figure) in the cross-section of the film: the change between the times t and $t + \mathrm{d}t$ in the volume contained between the cross-section at x and the contact line equals $Q(x)\mathrm{d}t$ (this is the volume injected in the same time interval). Let us assume, moreover, that the interface moves without deformation at velocity V: the preceding change in volume must also be equal to that $\xi(x)(V\,\mathrm{d}t)$ of a layer of fluid of thickness $V\,\mathrm{d}t$, located in the neighborhood of cross-section x, whence:

$$Q(x) = V\,\xi(x). \tag{8.48}$$

It follows therefore that the average velocity in section x defined by $V_m(x) = Q(x)/\xi(x)$ is constant with x and equal to V. In the lubrication approximation, the tangential stress $\eta\,\partial v_x/\partial z$ on the interface $z = \xi(x)$ vanishes (condition at a free surface); and, moreover, $v_x(0) = 0$. We will then have a velocity profile of the type $v_x(z) = A(x)(\xi(x) - z/2)z$. Integrating between 0 and $\xi(x)$ relative to z so as to calculate $Q(x)$, we find that:

$$v_x(x,\ z) = 3\,\frac{Q(x)}{\xi^3(x)}\left[\xi(x) - \frac{z}{2}\right]z. \tag{8.49}$$

We note that the velocity $v_x(x, \xi)$ of the fluid at the interface equals $3\ Q(x)/(2\ \xi(x))$: it is then higher than the average velocity $V_m(x) = V$ and also independent of x.

Let us now write that the power $\mathrm{d}E_{ts}/\mathrm{d}t$ given by Equation 8.47 equals the total power $\mathrm{d}E_\eta/\mathrm{d}t$ dissipated by viscosity in the flow corresponding to the velocity profile from Equations 8.49. From Equation 5.26, the dissipated power per unit volume is $\eta\ (\partial v_x/\partial z)^2$. We obtain the total dissipation $\mathrm{d}E_\eta/\mathrm{d}t$ (again per unit length in the transverse direction) by first integrating this expression between 0 and $\xi(x)$ with respect to z and then with respect to x. Let us now take $\xi(x) = \theta\ x$, which amounts to neglecting the curvature of the interface in the x-plane: assuming that the greatest part of the dissipation occurs very close to the contact line, the resulting error will be quite small. Using Equations 8.48 and 8.49, we then obtain in absolute magnitude:

$$\frac{dE_\eta}{dt} = \int 3\ \eta\ \frac{Q^2(x)}{\xi^3(x)}\ \mathrm{d}x = 3\ \eta V^2 \int \frac{1}{\xi(x)}\ \mathrm{d}x = 3\ \eta\frac{V^2}{\theta}\ \int_{x_m}^{x_M}\frac{1}{x}\ \mathrm{d}x. \tag{8.50}$$

Here, we needed to introduce an upper limit x_M and lower limit x_m, because of the logarithmic divergence of the integral as x approaches zero and infinity. We can assume that the upper limit x_M corresponds to a length of the order of the size of the droplet in the x-z plane, but we have a much more serious problem from the divergence of the dissipated power at very small distances from the contact line. This issue is, still at this time, the object of significant study and of numerical simulations on a molecular scale, and there is no exact solution presently available. Considering then x_m as an adjustable parameter of this model, we obtain:

$$\frac{\mathrm{d}E_{ts}}{\mathrm{d}t} = \gamma(1 - \cos\ \theta)V = \frac{\mathrm{d}E_\eta}{\mathrm{d}t} = 3\,\eta\ \frac{V^2}{\theta}\ \mathrm{Log}\left(\frac{x_M}{x_m}\right). \tag{8.51}$$

Our approach here, based on an estimate of the driving and dissipation effects, is only approximate. In fact, the assumption of a plane interface implies that there is zero capillary pressure difference between the sides of the interface, and, consequently, a constant pressure within the fluid. This contradicts the prediction (Equations 8.49) for the velocity profile, which requires a pressure gradient $\partial p/\partial x = -3\,\eta Q/\xi^3$. Thus, the interface needs to display a variable radius of curvature near the contact line so that the difference in capillary pressure can balance such gradients.

In the approximation of small contact angles, where $(1 - \cos\theta) \approx \theta^2/2$, we finally find *Tanner's equation*:

$$\theta^3 = 6\frac{\eta V}{\gamma}\mathrm{Log}\left(\frac{x_M}{x_m}\right) = 6\ Ca\ \mathrm{Log}\left(\frac{x_M}{x_m}\right). \tag{8.52}$$

The dimensionless *capillary number* $Ca = \eta V/\gamma$ indicates the relative importance of the effects due to the viscosity and those due to capillarity. The pressure differences of viscous and capillary origin are indeed respectively of the order of $\eta V/L$ and γ/L, so that their ratio is of the order of Ca, if the gradients of the velocity and the radii of the curvature of the interfaces have the same characteristic length L (if this were not the case, the ratio would still be of the order of Ca, but we would need to introduce a geometrical correction factor). The capillary number can also be considered as the ratio of the velocity V characteristic of the flow to a velocity γ/η characteristic of the fluid (of the order of 10^2 m/s for water). This result does not involve the value of the spreading parameter: this merely indicates the fact that the excess energy corresponding to a positive value of this parameter is assumed to be dissipated in the residual film, without influencing the dynamics of the macroscopic meniscus.

The experimental value of x_m (caption of Figure 8.10) is of the same order of magnitude as that resulting from the small-scale analysis of both the connection between the macroscopic meniscus and the precursor film, and the dissipation of energy in the precursor film. In this model, where the interface can no longer be considered as a sharp corner with angle θ, the transition region starts when the thickness of the film reaches a value smaller than a/θ (a is a length on an atomic scale). The corresponding value of the distance x_m is thus of order a/θ^2; this explains why x_m is large compared to atomic distances and accounts for the experimental value of x_m/x_M.

Figure 8.10 shows the experimental verification of Tanner's law, using measurements carried out by an optical method on a meniscus of silicone oil moving inside a capillary tube. The continuous curve displays the theoretical variation predicted by Tanner's equation (Equations 8.52) but with a multiplying factor equal to 9 instead of 6 as indeed predicted by more complete models. The ratio $\varepsilon = x_m/x_M$, is taken as equal to 10^{-4}, a value which gives the best agreement with the experimental points. These points follow very closely the theoretical prediction up to surprisingly large values of the angle θ_d, of the order of 100°. The corresponding value of x_m is of the order of 100 nm.

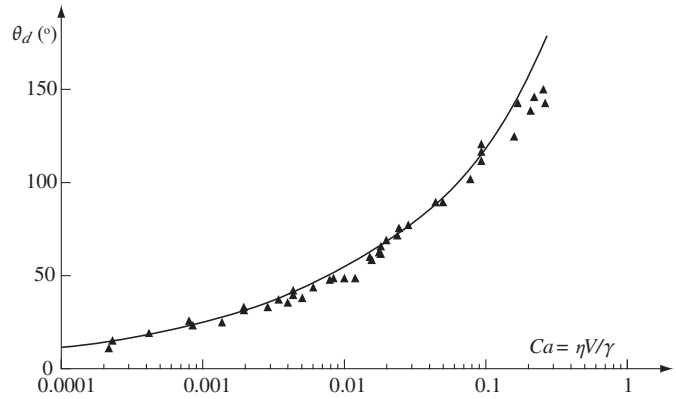

Figure 8.10 *Change in the contact angle as a function of the capillary number, Ca, for an interface silicone oil-air in a capillary tube, under conditions of complete wetting. (▲) Experimental data. (document courtesy of M. Fermigier and P. Jenffer). The solid curve is inferred from Tanner's law, using* $\varepsilon = x_m/x_M = 10^{-4}$

Contact angles under conditions of partial wetting

We can apply a similar approach to the case of partial wetting, so long as the wetting angle is not far from zero. The equations which we then obtain are more poorly obeyed than Tanner's law; we therefore use, in general, a rather empirical approach which generalizes this law. Other models involving molecular adsorption processes have also been suggested.

One of the difficulties involves the definition of the static contact angle, discussed in Section 1.4.3: depending on the direction of the motion of the contact line, the contact angle takes indeed general different values (for forward or backward motion) in the limit of small velocities.

8.2.3 Dynamics of the spread of droplets on a flat surface

Small droplets with complete wetting

Here, we are interested in the changes, as a function of time, of the radius of droplets of a non-volatile liquid which lie on a solid substrate, under conditions of total wetting. We will assume, just as we did in order to derive Tanner's law, that the dynamics of the droplet results from a continuous equilibrium between the viscous dissipation and the work done by capillary forces on the contact line. We assume (as we will discuss later), that it is enough to take into account the viscous dissipation in the region near the contact line (i.e. at distances small relative to the radius of curvature). We will thus apply to this three-dimensional system the equations which we have used above for the two-dimensional case of a straight contact line. More precisely, we assume that they continue to be valid so long as the radius of curvature of the interface is much greater than the thickness of the droplet.

Let us denote by Ω the volume of the droplet and assume that it keeps the shape of a spherical cap of height $h(t)$, with a radius of curvature $R(t)$ and with a contact radius $r_g(t)$ with the plane (Figure 8.11). We then have:

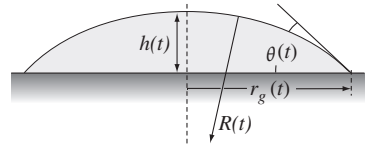

Figure 8.11 *Spreading of a droplet under the action of capillary forces*

$$\Omega = (\pi/4)\, r_g^3\, \theta. \tag{8.53}$$

Proof

We have an exact relationship $(2R - h)\, h = r_g^2$ (Figure 8.11) between the geometrical parameters. We obtain the volume of the spherical cap by integration from zero to $h(t)$ of $\pi\, r^2\, \mathrm{d}z = \pi(2R - z)\, z\, \mathrm{d}z$ (here r is the radius, expressed in terms of the same equation, of the horizontal cross-section of the cap at an arbitrary value of the height z, taken as positive downward from the top of the cap). We then obtain:

$$\Omega = \pi\left(R\, h^2 - \frac{h^3}{3}\right) \approx \pi\, R(t)\, h^2(t) = \frac{\pi}{2} r_g^2(t)\, h(t). \tag{8.54}$$

Moreover, we also have $h(t) = r_g(t)\, \tan(\theta/2)$ so that we obtain Equation 8.53 by assuming that the angle θ is much smaller than 1.

Combining Equations 8.52 and 8.53 and substituting $\mathrm{d}r_g/\mathrm{d}t$ for V, we obtain then:

$$\frac{\mathrm{d}r_g}{\mathrm{d}t} = \frac{\gamma}{\eta} \frac{1}{6\, \mathrm{Log}\left(\frac{x_M}{x_m}\right)} \left[\frac{4\Omega}{\pi r_g^3}\right]^3, \quad (8.55) \quad \text{thus:} \quad \left[r_g(t)\right]^{10} = \frac{5}{3} \frac{\gamma}{\eta\, \mathrm{Log}\left(\frac{x_M}{x_m}\right)} \left[\frac{4\,\Omega}{\pi}\right]^3 t. \tag{8.56}$$

We therefore predict a very slow growth, as $t^{1/10}$, of the radius of the droplet as a function of time. Because the product $r_g^3(t)\, \theta(t)$ is constant (Equation 8.53), $\theta(t)$ decreases as $t^{-3/10}$ under these circumstances. The numerical coefficients can be easily calculated by combining Equations 8.54 and 8.56. We note that the solution obtained here can only be approximate because we have assumed that the radius of curvature is constant along the interface, since it is taken as a spherical cap. Also, the pressure just below the free surface is constant along that surface: this in fact contradicts the existence of a spreading flow which leads to pressure gradients resulting from the viscosity (we have already discussed

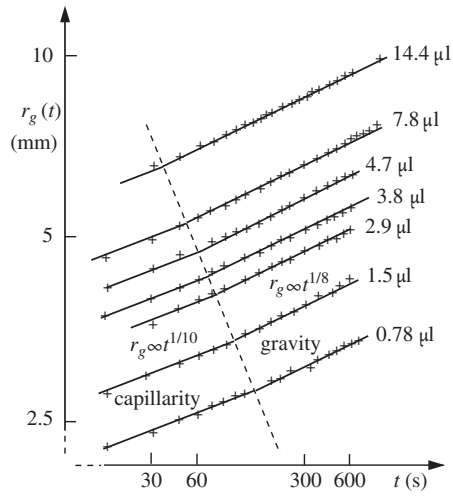

Figure 8.12 *Variation with time (in log-log coordinates) of the radius $r_g(t)$, for a series of droplets of silicone oil of variable volume* Ω, *(*$\eta = 0.02$ Pa.s, $\gamma = 20$ mN/m*), which are spreading on flat plates of hydrophilic glass. The dashed line indicates the boundary between the regimes dominated by gravity and by capillarity. The solid lines respectively to the right and to the left of the dashed line correspond to the change in the power-law of the exponents, from* 1/10 *and* 1/8. *(document courtesy of A.M. Cazabat, and M. Cohen Stuart)*

this concept when we dealt with Tanner's law). The exact solution is quite complicated: it predicts a similar dependence of $r_g(t)$ on the physical parameters, but with somewhat different numerical coefficients.

Figure 8.12 displays the variation as a function of time of the radius of a series of droplets of silicone oil lying on smooth plates of hydrophilic glass. The variation of $r_g(t)$ as $t^{1/10}$ is only observed at short times (to the left of the dashed line) when r_g is small enough so that the capillary effects dominate. At longer times, we enter into a regime dominated by gravity which is applicable to the droplets of larger diameter which we will now describe. We have in fact shown in Section 1.4.4 that it is the relative values of the radius r_g and of the capillary length which determine the relative importance of the capillary and gravity effects.

The gravitational spread of large drops

In this case, gravity plays a dominant role in determining at the same time the geometry of the drop and its dynamics. The drops can then be viewed as flat in the center region, with their curvature localized at the edges (Figure 8.13). We will first compare the energy dissipation per unit time due to the viscosity in the center region ($dE_{\eta cr}/dt$) to that near the contact line ($dE_{\eta cl}/dt$) which has already been calculated in the preceding case. Their ratio has the value:

$$\left[\frac{dE_{\eta cr}}{dt}\right] \Big/ \left[\frac{dE_{\eta cl}}{dt}\right] \approx \left[\frac{r_g\,\theta}{4\,h}\right] \Big/ \left[\mathrm{Log}\left[\frac{x_M}{x_m}\right]\right]. \tag{8.57}$$

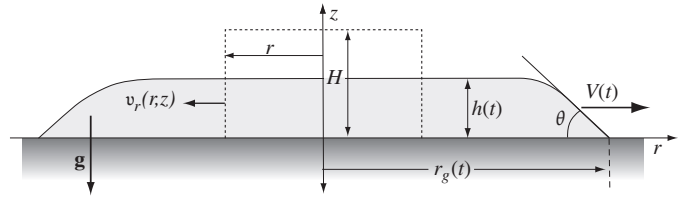

Figure 8.13 *Schematic diagram of a large-radius drop spreading out under the effect of gravity*

Within a logarithmic coefficient, this ratio is of the order of magnitude of the ratio of the radius r_g of the drop to the width ($\approx h/\theta$) of the transition zone between the contact line and the flat center region of the drop. Thus, for drops of outer radius r_g large relative to h/θ, the dissipation by viscosity in the flat region of the drop ends up being the dominant one, in contrast to the small droplets discussed previously for which the dissipation near the contact line is the most significant.

Proof

Let us assume that, in the central region, the drop has a thickness $h(t)$ independent of the distance r to the axis. Let us analyze the conservation of the mass of liquid in a cylinder of radius r, with the same axis as the drop, and of constant height H always larger than the thickness of the drop ($H>h(t)$). The volume rate of flow $Q(r)$ through the walls of this cylinder is opposite to the change per unit time of the amount of fluid inside, so that:

$$Q(r) = 2\pi\, r h\, V_m(r) = -\pi r^2 \frac{dh}{dt} \quad (8.58a) \qquad \text{or:} \quad \frac{1}{h}\frac{\mathrm{d}h}{\mathrm{d}t} = -2\frac{V_m(r)}{r} = \text{cst with } r, \quad (8.58b)$$

where $V_m(r)$ is the average, over the thickness h of the drop, of the radial velocity $v_r(r,z)$ of the fluid. Moreover, as in Equations 8.48, the average velocity $V_m(r_g)$ equals the spread velocity $V(r_g) = \mathrm{d}r_g/\mathrm{d}t$ at the edge of the drop. Combining this result with Equations 8.58b, applied to the radii r and r_g, we obtain:

$$V_m(r) = V_m(r_g)\frac{r}{r_g} = \frac{dr_g}{dt}\frac{r}{r_g}. \quad (8.59)$$

Just as in Equation 8.49, the velocity profile $v_r(r,z)$ in the thickness of the drop is a half parabola with a velocity maximum equal to $3V_m(r)/2$ at the interface. We then find that the absolute value of the viscous energy dissipation per unit time $\mathrm{d}E_{\eta cr}/\mathrm{d}t$ in the flat center region of the drop, with radius approximately equal to r_g, satisfies:

$$\frac{\mathrm{d}E_{\eta cr}}{\mathrm{d}t} = \eta \int_0^{r_g} 2\pi\, r\, \mathrm{d}r \int_0^{h(r)} \left(\frac{\partial v_r}{\partial z}\right)^2 \mathrm{d}z = \frac{3}{2}\pi\,\eta\, V^2\, \frac{r_g^2}{h} = \frac{3}{2}\pi\,\eta \left(\frac{dr_g}{dt}\right)^2 \frac{r_g^2}{h}. \quad (8.60a)$$

Applying Equations 8.51 along the perimeter $2\pi r_g$ of the drop, we find the energy $\mathrm{d}E_{\eta cl}/\mathrm{d}t$ dissipated by the viscosity per unit time, in the area of the contact line:

$$\frac{\mathrm{d}E_{\eta cl}}{\mathrm{d}t} = 6\pi\,\eta\, r_g \frac{V^2}{\theta}\mathrm{Log}\left(\frac{x_M}{x_m}\right). \quad (8.60b)$$

We then recover Equation 8.57 by taking the ratio of these two dissipation terms.

We determine now the spreading equation for drops, for the case where gravity is the dominant force (Figure 8.13). Just as in the previous case, we assume that the liquid in question is non-volatile, in order to avoid evaporation phenomena which, often accompanied by changes in the surface tension, create additional flow by virtue of the Marangoni effect (we will be discussing this in Section 8.2.4, which follows).

We estimate the spreading law by assuming that the thickness of the drop is uniform all over its surface. The dissipation of energy through viscosity must, at every instant

of time, correspond to the change in potential energy of the drop which has the value: $(\mathrm{d}/\mathrm{d}t)[(\pi/2)\rho\, g\, r_g^2 h^2]$. Moreover, the volume $\Omega = \pi\, r_g^2 h$ of the drop is constant. We thus have, using Equations 8.60a to evaluate the viscous dissipation, the following energy balance:

$$\frac{\mathrm{d}}{\mathrm{d}t}\left(\frac{\pi}{2}\rho\, g\, r_g^2 h^2\right) = -\frac{3}{2}\eta\,\pi\left(\frac{\mathrm{d}r_g}{\mathrm{d}t}\right)^2 \frac{r_g^2}{h}. \tag{8.61}$$

We can evaluate $r_g(t)$, in the same manner, but with more precise coefficients, by assuming that the thickness $h(r, t)$ of the film is no longer exactly constant as a function of the distance from the axis, but is described by a self-similar profile; more precisely, it must satisfy a relation of the type $h(r, t) = h(0, t)\, f(r/r_g(t))$ in which $r_g^2(t)\, h(0, t)$ is constant with time in order to keep constant the liquid volume, and $f(x) = 0$ for $x > 1$.

Let us now substitute for h its value as a function of Ω and r_g. We then obtain:

$$r_g^7 \frac{\mathrm{d}r_g}{\mathrm{d}t} = \frac{2\,\Omega^3}{3\,\pi^3}\frac{\rho\, g}{\eta}, \qquad (8.62) \qquad \text{so that:} \qquad r_g(t) = \left(\frac{\Omega}{\pi}\right)^{\frac{3}{8}}\left(\frac{16}{3}\frac{\rho\, g\, t}{\eta}\right)^{\frac{1}{8}}. \tag{8.63}$$

In this way, we then predict (assuming that the radius of the drop is zero at time $t = 0$), a growth of the drop as $t^{1/8}$, instead of $t^{1/10}$ in the previous case. This result is in agreement with the growth at long times, which we observe on the curves in Figure 8.12.

The spreading behavior as $t^{1/8}$ and $t^{1/10}$ represents two limiting cases, applicable to drops spreading under conditions of complete wetting. Other types of spreading behavior (as $t^{1/4}$) are observed for flow on a rotating plate, or on some surfaces with roughness. Adapting these models to the geometries and properties of more complex fluids has very important applications to the spreading of decorative or protective coatings. Another important practical problem, which we will not discuss here, is the appearance of interfacial instabilities in flowing films, which can be brought on by deformations, often very significant, of the contact line, or by changes in the depth.

8.2.4 Flows resulting from surface-tension gradients: the Marangoni effect

Principle of the Marangoni effect

Gradients in the surface tension due to changes in temperature or in the concentration of solutes (e.g., affecting surface tension) can create surface stresses and cause fluid motion. Fluid flow resulting from such stresses is known as the *Marangoni effect*; this is also known as the *thermo-capillary* effect when it results from temperature gradients.

Thus, if a layer of water covers a surface, and a piece of soap touches a point on that surface, we see this part of the surface "drying out" (Figure 8.14): the surface tension is indeed locally reduced and the forces due to surface tension become unbalanced. We thus have flow toward the neighboring regions where the surface tension is unchanged (this can be visualized by the motion of dust particles initially present on the surface).

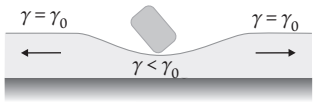

Figure 8.14 *Deformation of a fluid layer by the local addition of a small amount of tensioactive product*

Such motion of the fluid can also be due to variations in the temperature T from one point to another of a liquid-air or liquid-liquid interface. As shown in Section 1.4.1, the surface tension coefficient depends on temperature according to an equation which, for moderate changes in temperature, takes on the linear form:

$$\gamma(T) = \gamma(T_0)\,(1 - b\,(T - T_0)). \tag{8.64}$$

A temperature gradient parallel to the surface of a liquid causes a tangential stress on it (Figure 8.15 below). Along a strip of width δx, the surface tension forces are no longer in balance. The resultant force is directed toward the regions of lower temperature. Corresponding to a temperature gradient $\mathrm{d}T/\mathrm{d}x$, there is a surface-tension gradient equal to:

$$\frac{\mathrm{d}\gamma}{\mathrm{d}x} = \frac{\mathrm{d}\gamma}{\mathrm{d}T}\frac{\mathrm{d}T}{\mathrm{d}x} = -b\,\gamma(T_0)\left(\frac{\mathrm{d}T}{\mathrm{d}x}\right). \tag{8.65}$$

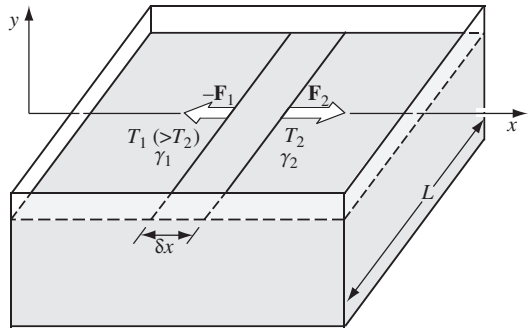

Figure 8.15 *The appearance of tensile stresses at the free surface of a liquid as a result of a horizontal temperature gradient*

This gradient causes a stress $\sigma_{xy}^{(\gamma)}$, in the x-direction, on the surface element $L\,\delta x$, where:

$$\sigma_{xy}{}^{(\gamma)} = \frac{F_2 - F_1}{L\,\delta x} = \frac{(\gamma_2 - \gamma_1)L}{L\,\delta x} = \frac{\mathrm{d}\gamma}{\mathrm{d}x} = -b\,\gamma\,(T_0)\left(\frac{\mathrm{d}T}{\mathrm{d}x}\right). \tag{8.66}$$

The negative sign appearing in $\sigma_{xy}^{(\gamma)}$ indicates the fact that the resultant tension (and the flow that results from it) acts in the direction of lower temperature.

Flow created in a horizontal liquid layer by a temperature gradient

The stress $\sigma_{xy}^{(\gamma)}$ on the interface due to the surface-tension gradient will generate a flow of velocity $v_x(y)$ which, in turn, will induce a viscous friction stress $\sigma_{xy}^{(\eta)} = -\eta\,(\partial v_x/\partial y)$ at the interface. For a free, plane, gas-liquid interface, the total tangential stress must vanish so that the stresses $\sigma_{xy}^{(\gamma)}$ and $\sigma_{xy}^{(\eta)}$ must balance each other. We then have:

$$\sigma_{xy}^{(\gamma)} + \sigma_{xy}^{(\eta)} = -b\,\gamma\,(T_0)\,\frac{\mathrm{d}T}{\mathrm{d}x} - \eta\left(\frac{\partial v_x}{\partial y}\right)_{\text{interface}} = 0. \tag{8.67}$$

Let us now calculate the resultant flow-profile in a fluid film bounded from below by a solid horizontal plane $y = 0$, of average thickness a, and extending infinitely in the z-direction (Figure 8.16). We assume, as in the previous sections, that the flow is one-dimensional, the only non-zero component being $v_x(y)$.

The pressure gradient in the y-direction satisfies: $(\partial p/\partial y) = -\rho g$. Let us assume that, at the onset, the upper surface is perfectly horizontal, that the density of the fluid is not

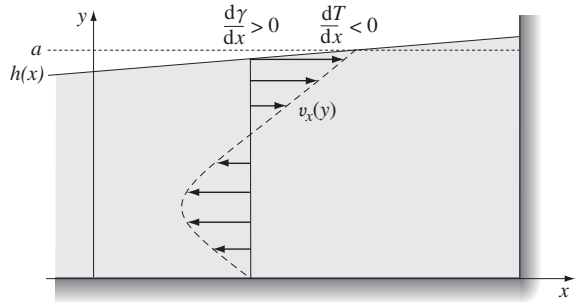

Figure 8.16 *Velocity profile within a finite-length fluid film, in the presence of a horizontal temperature gradient, which causes a recirculating flow due to the Marangoni effect. The pressure gradient resulting from the parabolic velocity profile causes a deformation of the free upper surface*

a function of temperature, and that this density is uniform throughout the depth h. The pressure satisfies everywhere the equation:

$$p = p_{atm} + \rho\, g\, (a - y). \tag{8.68}$$

The pressure is then independent of x and the x-component of the equation of motion reduces to:

$$\eta \frac{\partial^2 v_x}{\partial y^2} = 0. \tag{8.69}$$

The velocity v_x then varies linearly with y, just as for simple shear flow. Making use of Equations 8.67, we find:

$$v_x(y) = -\frac{b\ \gamma(T_0)}{\eta} \left(\frac{\mathrm{d}T}{\mathrm{d}x}\right) y. \tag{8.70}$$

In a real situation, the film is of finite length in the x-direction. As a result, the fluid piles upon the side towards which the flow is directed leading to a gradient in the thickness $h(x)$ of the film. Let $\mathrm{d}h/\mathrm{d}x$ be the slope of the free surface ($dh/dx \ll 1$); the flow remains quasi one-dimensional and the vertical pressure gradient is still equal to $-\rho g$. The only effect of the slope in the surface is thus to induce a horizontal pressure gradient $\rho g(\mathrm{d}h/\mathrm{d}x)$. Under stationary conditions, the latter creates a subsurface counterflow which exactly compensates the shear flow near the surface, to give a zero net-flow rate. The profile of the interface then satisfies the condition:

$$h^2(x) - h^2(x_0) = -\frac{3b\,\gamma(T_0)}{\rho g} \left(\frac{\mathrm{d}T}{\mathrm{d}x}\right) (x - x_0). \tag{8.71}$$

The phenomenon we have just described can be easily observed by bringing the tip of a hot soldering iron near a water surface; a dip can be seen in the surface just below the tip.

Proof

The equation of motion corresponding to the overall stationary state can be written:

$$\eta \frac{\partial^2 v_x}{\partial y^2} = \rho\, g\, \frac{\mathrm{d}h}{\mathrm{d}x}.$$

Integrating, with the conditions:

$$\int_0^{h(x)} v_x(y)\ \mathrm{d}y = 0 \quad \text{and:} \quad v_x(0) = 0, \qquad \text{we obtain:} \quad v_x = \frac{\rho g}{\eta} \frac{\mathrm{d}h}{\mathrm{d}x} \left(\frac{y^2}{2} - \frac{y\,h}{3}\right). \tag{8.72}$$

This flow is therefore a superposition of a shear flow and a Poiseuille flow. We can find the value of $\mathrm{d}h/\mathrm{d}x$ by using again the condition of Equations 8.67 for the surface stress, thus:

$$h \frac{\mathrm{d}h}{\mathrm{d}x} = -\frac{3}{2} \frac{b\,\gamma(T_0)}{\rho g} \left(\frac{\mathrm{d}T}{\mathrm{d}x}\right). \tag{8.73}$$

Equation 8.71 results from this, by integration.

Surface-tension gradients resulting from temperature differences are the basis of numerous hydrodynamic instabilities. Among the best-known of these is the *Bénard-Marangoni instability* of a horizontal fluid layer with a free surface, heated from below. We will discuss

in more detail, in Section 11.3.1, this phenomenon which causes the appearance of a hexagonal lattice of convection cells. We also observe the rise of a liquid film when we dip a vertical plate, heated at the top, into the liquid. Finally, liquid drops begin to move if they are placed on a plate or on a wire where there exists a temperature gradient.

In industrial applications, flow resulting from surface gradients of thermal origin can have significant practical importance. For example, this occurs in the case of very pure single crystals produced by cooling in the presence of temperature-gradients: defects can appear because of this flow. The motion of bubbles resulting from such gradients can also greatly influence thermal transfer for boiling occurring along a heated wall.

Marangoni effect resulting from changes in the chemical composition

We can cause changes in the surface tension of a fluid by adding tensioactive compounds: one example is that of the amphiphilic molecules that we mentioned in Section 1.4.1, which can significantly reduce the surface tension when they are present along an interface. A concentration gradient of such molecules along a gas-liquid or liquid-liquid interface leads to a surface tension gradient which will result in Marangoni flow.

A spectacular example of this is the phenomenon of "*wine legs*" or *"tears of wine*" which can be seen in a glass partly filled with wine having a sufficiently high alcohol content. Swirling the glass creates a liquid film along the walls, above the surface of the wine. We see the liquid film rise, first creating a bulge near the top, followed by the appearance of droplets which fall regularly downward after a certain amount of time.

This phenomenon is the result of the decrease in surface tension of a water-alcohol solution (the wine!), as the concentration of alcohol increases. The evaporation of the alcohol from the liquid film leads to an increase in its surface tension, and causes the rise of the fluid film above the free surface where the surface tension is unchanged. In the bulge, the evaporation diminishes and the gradients in the surface tension can no longer balance the effects of gravity on the droplets, which fall in *"tears of wine"*, also called *"wine legs"* (Figure 8.17).

We have seen at the beginning of this section the example of putting a small amount of soap on a thin, horizontal layer of water: the water *"dessicates"* because the surface tension is highly decreased at this point, and all of the liquid is pulled toward other regions. This phenomenon is found to have practical applications in the drying of certain fragile and very expensive objects, such as the disks (*wafers*) of silicon used in microelectronic applications (in this last case, the process involves blowing alcohol vapor or a similar compound).

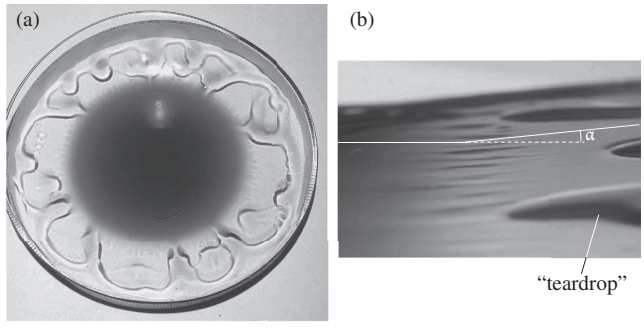

Figure 8.17C *(a) Top view of the rise of a liquid along the walls of a glass due to the Marangoni effect, and of the fall of the liquid with a lower alcohol concentration in the form of "teardrops" or "wine legs." (b) Close-up side view of a model experiment which displays this phenomenon. One pulls a plate inclined at an angle* α *relative to the horizontal from the water-alcohol mixture: this creates on the plate a fluid film which drops back as legs or teardrops. The narrower transverse ridges correspond to a different flow instability (documents courtesy of J. Bush and P. Hosoi, MIT)*

8.3 Falling liquid cylindrical jet

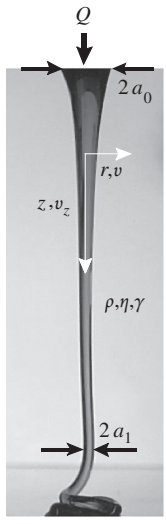

Figure 8.18 *Jet of viscous fluid falling from an orifice. The jet falls onto a plane at the bottom of the figure, which leads to the observed coiling; this coiling is not discussed here, and we will interest ourselves only in the straight portion of the jet (image courtesy of N. Ribe)*

In every example discussed so far in this chapter, the flow occurred in the presence of one or more walls: in the stationary flow regime, forces due to gravity or to the pressure gradients could then be balanced by the viscous stresses on the wall(s).

This is no longer the case when we have a free jet flowing from an opening, as shown in Figure 8.18. The viscous shear stress σ'_{zr} at the free surface of the jet ($r = a(z)$) can, in this case, be considered to be negligible: this leads to the conclusion that the radial gradient of the velocity component v_z also vanishes near the surface (Section 4.3.2, Equation 4.37). The absence of this viscous shear stress component σ'_{zr} which might otherwise cause radial changes in the velocity of the jet leads us to assume that v_z is independent of r.

Even if the cross-section of the jet changes slowly with distance, and the flow is quasi-parallel, the assumptions of the lubrication approximation must be entirely revised: this approximation was indeed based on the existence of equilibrium between the shear stresses and either the pressure gradients or gravity.

Other viscous terms which we have so far neglected relative to σ'_{xr} need to be taken into account: these are, specifically, the diagonal components of the viscous shear tensor which oppose the stretching of the jet as the fluid velocity changes in the x-direction. In the present case, the components which have to be taken into account include: $\sigma'_{zz} = 2\,\eta\,\partial v_z/\partial z$ and $\sigma'_{rr} = 2\,\eta\,\partial v_r/\partial r$ (Chapter 4, appendix 4A.2).

8.3.1 Stable flow regime

Equations of motion

In the one-dimensional model discussed here, the change in the cross-section $A(z) = \pi\, a^2(z)$ and the velocity $v_z(z)$ of the jet satisfy the following equation of motion proven below:

$$\rho g A(z) = \rho A(z) \left(v_z(z) \frac{\partial v_z(z)}{\partial z} \right) + \pi\gamma \frac{\partial a(z)}{\partial z} - 3\eta \frac{\partial}{\partial z} \left[A(z) \frac{\partial v_z(z)}{\partial z} \right]. \tag{8.74}$$

This equation of motion expresses the fact that the force of gravity is balanced by a combination of three terms:

- the inertial term, indicating the acceleration of the fluid along its trajectory;
- the change in the z-direction of the capillary pressure;
- viscous stresses related to the lengthening of the jet in the z-direction, to the decrease of its cross-section and to the resulting change in velocity.

Proof

Let us integrate with respect to r the condition of incompressibility $\nabla \cdot \mathbf{v} = 0$ in cylindrical coordinates (Chapter 4, appendix 4A.2), taking into account the finite velocity v_r at $r = 0$ and the fact that v_z, and thus its gradient $\partial v_z/\partial z$, are not functions of r. We then obtain:

$$v_r = -\frac{r}{2} \frac{\partial v_z}{\partial z}, \tag{8.75}$$

from which we infer:

$$\sigma'_{rr} = 2\eta \frac{\partial v_r}{\partial r} = -\,\eta\, \frac{\partial v_z}{\partial z} = -\frac{\sigma'_{zz}}{2}. \tag{8.76}$$

In order to ensure that the jet is in mechanical equilibrium in the transverse direction, we must have $p - \sigma'_{rr}$ independent of r. Since, from Equations 8.76, σ'_{rr} must be independent of

r, the same needs to be true regarding the pressure. On the other hand, if p is the pressure inside the fluid at the level of the interface, we must also have:

$$p - \sigma'_{rr} = p_{atm} + \frac{\gamma}{a(z)}, \qquad \text{i.e.:} \qquad p = p_{atm} + \frac{\gamma}{a(z)} - \eta\,\frac{\partial v_z}{\partial z}. \quad (8.77)$$

We assume, moreover, that the flow is stationary; the rate of flow Q of the fluid in the jet is:

$$Q = \pi\, a^2(z)\, v_z(z) = A(z)\, v_z(z) \quad (8.78)$$

must be constant as a function of z and of t in order to ensure the conservation of mass ($A(z)$ is the cross-section of the jet at the distance z). Let us now write Equation 5.10 for the conservation of momentum in a slice of the jet located between the cross-sections z and $z + \delta z$:

$$\rho\, g\, A\, \delta z = \left[\rho\, Q\, v_z(z) + (p(z) - p_{atm})A(z) - \sigma'_{zz}\, A(z)\right]_z^{z+\delta z}. \quad (8.79)$$

Rewriting this equation in differential form, and using Equations 8.75, 8.77 and 8.78, we obtain Equation 8.74.

We assume, first of all, that the change in capillary pressure has a negligible effect, and we will look for the laws involving changes in the two limiting cases, where either the inertial term or the viscous term dominate.

Inertial regime

Equation 8.74 reduces to: $$g = v_z \frac{\partial v_z}{\partial z},$$

so that, by integration: $$v_z^2(z) - v_{z0}^2 = 2\,gz. \quad (8.80)$$

We recognize that this is the change in velocity with distance of an object in free fall: this is a logical result since the only frictional forces are of viscous origin, and, here, we assume they are negligible. When $v_z(z) \gg v_{z0}$ the velocity thus increases as the square root of the distance ($v_z(z) = \sqrt{2\,g\,z}$).

Viscous regime

Equation 8.74 becomes: $$\rho\, g A(z) = -3\,\eta\,\frac{\partial}{\partial z}\left[A(z)\frac{\partial v_z(z)}{\partial z}\right]. \quad (8.81)$$

From this, we infer the following variations of the flow velocity and the cross-section, as functions of z:

$$v_z(z) = \frac{g}{6\nu}\,(z - z_i)^2 \quad (8.82a) \qquad \text{and} \qquad A(z) = \frac{6\nu\, Q}{g}(z - z_i)^{-2}. \quad (8.82b)$$

We can then determine z_i (< 0) from the value v_{z0} of the flow velocity at $z = 0$. For $v_z \gg v_{z0}$, the velocity increases as the square of the distance ($v_z = g\,z^2/6\nu$).

Proof

Gravity is compensated, in the present case, by the viscous stresses resulting from the stretching of the jet. Let us assume that, as in the previous situation, v_z has a power-law dependence on z or, more precisely, on $(z - z_i)$, where z_i is an arbitrary origin so that $v_z = C_\eta\,(z - z_i)^\alpha$: this implies that $A = (Q/C_\eta)\,(z - z_i)^{-\alpha}$. Inserting this into Equations 8.81, we obtain $(z - z_i)^{2-\alpha} = 3\,\nu\,\eta\,C_\eta/g$, which requires $\alpha = 2$ and $C_\eta = g/6\nu$. This leads to Equations 8.82a and 8.82b.

For an injection orifice of diameter d, this self-similar power-law solution is only valid far downstream of the orifice, when the cross-section $A(z)$ of the jet is small compared to its initial value $\pi d^2/4$. Combining this condition with Equation 8.82a, we obtain: $z - z_i \gg \sqrt{(24/\pi)\,(\nu\,Q/(d^2 g))}$.

Transition from the viscous to the inertial regime

The viscous regime is found in the start-up phase where the viscous forces maintain a low flow velocity. Subsequently, the inertial effects take over.

Let us evaluate, in the viscous regime and where $v_z \gg v_{z0}\,(z \gg z_i)$, the change with distance in the inertial and viscous terms in Equation 8.74, by means of Equations 8.82a and 8.82b. We find:

$$\rho\,A\left(v_z\frac{\partial v_z}{\partial z}\right) \simeq \frac{\rho\,Q\,g\,z}{3\,\nu} \qquad (8.83a) \qquad \text{and:} \qquad -3\,\eta\,\frac{\partial}{\partial z}\left[A\frac{\partial v_z}{\partial z}\right] \simeq \frac{6\,\eta\,Q}{z^2}. \qquad (8.83b)$$

The ratio of the inertial to the viscous term is thus of the order of $g\,z^3/(18\,\nu^2)$: the inertial term increases with the distance while the viscous term decreases (because of the decrease of $A(x)$). The distance z_c corresponding to the transition (ratio of the order of unity) is then:

$$z_c \cong \left(\frac{18\,\nu^2}{g}\right)^{1/3} \qquad (8.84a) \qquad \text{from which we infer:} \qquad v_z(z_c)\,z_c \cong 3\,\nu. \qquad (8.84b)$$

We find Equation 8.84b by writing Equation 8.82a for $z = z_c$, assuming $v_z \gg v_{z0}$, and then multiplying both sides by ${z_c}^2$.

In order for the viscous regime to extend throughout the length of the jet, we must have $z_c \geq L$: in the limit $z_c = L$, we then have: $v_L\,L \cong 3\,\nu$. The Reynolds number $Re_L = v_L\,L/\nu$, based on the length of the jet must be at most of the order of unity.

Even for a slow change of radius as a function of the distance (quasi-parallel flow), the viscous terms will only be dominant, in a real situation, if we use very viscous fluids in order, from Equation 8.84a, to satisfy the condition $z_c \geq L$.

In the case of water ($\nu \approx 10^{-6}$ m^2/s), one finds $z_c \approx 0.12$ mm which makes any experimental observation extremely difficult. In order to reach a value of the order of 0.1 m we need a viscosity around 2.5×10^{-2} m^2/s, i.e., about 25,000 times the viscosity of water.

This condition is much stricter than that for the lubrication approximation, for flow in the presence of a wall, which here would be $v_L a_0/\nu < 1/\theta \approx \mathrm{L}/a_0$; this is equivalent to $Re_L < (\mathrm{L}/a_0)^2$ where $(L/a_0)^2 \gg 1$. This result reflects the much smaller values of the viscous terms in the absence of a wall: these terms then result uniquely from the stretching of the jet, which leads to longitudinal and transverse flow-velocity gradients which are much smaller than for a shear flow in the presence of a wall.

8.3.2 Capillary effects and Rayleigh-Plateau instability of the jet

Until now, we have neglected surface-tension effects in the flow of vertical jets. In fact, for very viscous fluids, the flow described just above remains stable. On the other hand, for liquids with low viscosity, such as water, the effect of surface tension can lead to an instability and to the formation of drops; we can easily observe this by looking at the evolution, as a function of distance, of a jet of water, originally cylindrical (Figures 8.19a,b).

In order to explain this instability, known as the *Rayleigh-Plateau instability*, let us calculate the changes in the capillary pressure resulting from a deformation of the external surface of an originally cylindrical jet of liquid. When no deformation is present, the capillary pressure difference p_{cap} between the inside of the jet and the (constant) atmospheric pressure p_{at} outside satisfies $p^0_{cap} = \gamma/R_0$. Let us assume now that the jet remains axially

symmetric, and that its local radius, $R(z)$ is modulated sinusoidally in the z-direction of its axis (Figure 8.19b):

$$R(z,t) = R_0 + h(t)\cos kz. \tag{8.85}$$

Here, we assume that the velocity profile in the jet is uniform and we study the deformations in a reference frame moving at the corresponding (gravity is assumed to have no influence on the instability). We also assume that $h(t) \ll R_0$ and that the slope of the interface remains small ($\mathrm{d}R/\mathrm{d}z \ll 1$). The variation $\Delta p_{cap}(z,t) = p_{cap}(z,t) - p^0_{cap}$ of the capillary pressure difference due to the deformation is:

$$\Delta p_{cap}(z,\ t) = \gamma\ h(t)\ \cos kz \left(k^2 - \frac{1}{R_0^2}\right). \tag{8.86}$$

Justification

The pressure difference $p_{cap}(z)$ is determined from the Young-Laplace law (Equation 1.58), in terms of the sum of the contributions of the two radii of curvature R_1 and R_2 of the jet surface respectively in planes containing and perpendicular to the axis. We then obtain:

$$\begin{aligned} p_{cap}(z,t) &= \gamma\left(\frac{1}{R_1} + \frac{1}{R_2}\right) = \gamma\left(-\frac{\partial^2 R(z,t)}{\partial z^2} + \frac{1}{R(z,t)}\right) \\ &= \gamma\left(k^2 h(t)\cos\ kz + \frac{1}{R_0 + h(t)\cos\ kz}\right), \end{aligned} \tag{8.87}$$

Expanding the last term on the right-hand side in terms of h/R_0 and substracting p^0_{cap}, we obtain Equation 8.86.

When $k^2 - 1/R_0^2 < 0$, Δp_{cap} becomes negative in the regions where $R(x) > R_0$ ($\cos kz > 0$) and, in contrast, positive for $R(z) < R_0$ ($\cos kz < 0$). Since the pressure inside the non-deformed jet is constant (and equal to $p_{at} + \gamma/R_0$), the pressure in the regions where the radius of the jet increases due to the deformation will be larger than in those where it decreases. The flow resulting from these pressure differences thus reinforces the instability. The absolute amplitude of these pressure changes is greatest when $|k| \ll 1/R_0$ and decreases when k approaches $1/R_0$.

This larger value of the changes in capillary pressure as a function of z for long-wavelength deformations might seem paradoxical: capillary effects generally increase indeed with the curvature of the interfaces. But, here, the contribution to the Young-Laplace law of the curvature in planes containing the axis (k^2 term in Equations 8.86) stabilizes the interface; it is the curvature in the planes normal to the axis which is destabilizing (term varying as $-1/R_0^2$). It is thus logical that the destabilising capillary pressure is highest when the first term almost vanishes, for $k \to 0$.

On the other hand, the change as a function of k of the rate of increase σ does not depend only on Δp_{cap} but also on the fact that the time for transfering matter between the regions of smaller and larger radii acts over a distance of the order of a half wavelength: the decrease in this distance as k increases must then, to the contrary, lead to an increase in σ. The approximate estimate of σ (carried out below) for an inertial flow:

$$\sigma^2 \propto k^2 R_0^2 \left(1 - k^2 R_0^2\right) \tag{8.88}$$

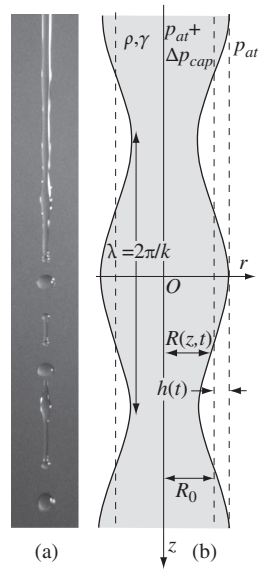

Figure 8.19C *Destabilization, by the Rayleigh-Plateau mechanism, of a vertical cylindrical liquid jet. a) experimental observation of the development of the instability, followed by the formation of drops (document courtesy of J. Aristoff and J. Bush, MIT); b) Schematic diagram for the development of the instability*

combines these two effects. This rate of increase is only positive if $k < 1/R_0$ (unstable case), and has a maximum when $k = 1/(R_0\sqrt{2}) \approx 0.7/R_0$: this value is quite close to that experimentally observed, and corresponds to a wavelength of 1.4 times the perimeter of the jet.

This last result is applicable to numerous instabilities which display a range of unstable wavelengths: the dominant instability is that of the wavelength for which the rate of growth is a maximum. Moreover, the simple model which we discuss here takes no account of the effects of the viscosity or of the average flow rate.

For highly viscous fluids, the Rayleigh-Plateau instability can still be observed, because the changes in the capillary pressure related to the deformations of the interface (Equation 8.86) remain the same. In contrast, Equation 8.88 is no longer valid because the development of the instability then results from the equilibrium between the capillary and the viscous forces.

Justification of Equation 8.88

In the cases for which the instability is best visible (fluids with small viscosity), we are generally in an inertial regime for which the effect of viscosity can be neglected: the acceleration $\partial v_z/\partial t$ of the fluid is then proportional to the pressure gradient in the z-direction. Assuming that this pressure gradient is uniform over the cross-section and equal to the capillary-pressure gradient, and that the velocity is also uniform, we have: $\rho\ \partial v_z/\partial t \approx -\partial \Delta p_{cap}/\partial z$. Using Equation 8.86 to estimate Δp_{cap}, the corresponding flow rate $Q(z,\ t)$ satisfies:

$$\frac{\partial Q(z,\ t)}{\partial t} \approx -\frac{\pi R_0^2}{\rho}\frac{\partial \Delta p_{cap}(z)}{\partial z} = \frac{\pi\,\gamma\,h(t)\ R_0^2}{\rho}\ \sin kz\ k\left(k^2 - \frac{1}{R_0^2}\right). \tag{8.89}$$

The conservation of the flow rate of fluid can be written locally for a given z in the form:

$$2\pi\ R_0 \cos kz\ \frac{\mathrm{d}h(t)}{\mathrm{d}t} = -\frac{\partial Q}{\partial z}, \tag{8.90}$$

The Rayleigh-Plateau instability can also be observed in the case of some, very soft, solids, such as gels. All solids are characterized by a surface energy: in contrast to liquids, the corresponding forces are, however, generally negligible in comparison with the elastic forces. Their ratio can be characterized by the length $h = \gamma/E$, where γ is the surface energy and E is Young's modulus (the ratio of the stress F/S to the resulting relative deformation $\Delta L/L$). For iron, for example, this length is 3×10^{-13} m and the surface energy has no significant effect on deformations on this scale. This is no longer the case for gels for which Young's modulus has a value of a few Pa (instead of $\approx 2 \times 10^{11}$ Pa for iron): the length h is then a few mm. Surface-tension forces are then sufficently great to result in a Rayleigh-Plateau instability (but, in contrast, the elastic forces can prevent the breaking up into droplets).

where the left-hand side represents the change with time of the cross-section of the jet (again when $h \ll R_0$). Taking the derivatives of Equations 8.89 and 8.90 respectively with respect to z and to t and setting the results equal, we obtain after dividing both sides by $2\pi\ R_0 h(t)$ cos kz:

$$\frac{1}{h(t)}\frac{d^2h(t)}{dt^2} \approx \frac{\gamma}{2\,\rho\,R_0^3}\ k^2R_0^2\left(1 - k^2R_0^2\right) \tag{8.91a}$$

or:

$$\sigma^2 \approx \frac{\gamma}{2\,\rho\ R_0^3}\ k^2\ R_0^2\ (1 - k^2R_0^2), \tag{8.91b}$$

assuming that $h(t)$ increases with time as $\exp(\sigma t)$. The exponential growth coefficient σ then satisfies Equations 8.88. If we take into account the pressure and radial velocity gradients, we obtain a similar result, where the factor $k^2R_0^2/2$ is replaced by a function $f(kR_0)$ whose maximum corresponds to $k = 0.697/R_0$, remarkably close to the value obtained from the simple approximation above.

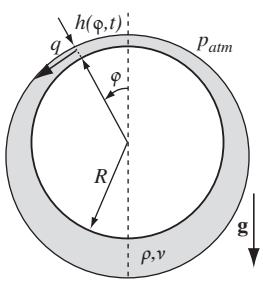

EXERCISES

In the following exercises, the lubrication approximation (see Section 8.1.2) is assumed to be valid and the thickness of the liquid films is assumed to vary slowly with distance parallel to the flow.

1) **Flow of a fluid layer around a horizontal cylinder**

A horizontal circular cylinder of radius R and axis along z (see in the margin), is coated externally by a layer of a Newtonian fluid of initial thickness $h_0 \ll R$ constant with respect to the coordinates z and φ (using cylindrical coordinates r,φ,z). This represents,

for instance, the painting of a tube by means of a brush: we are interested in the subsequent flow of the paint leading to azimuthal variations of its thickness. Show that the influence of the pressure gradients on the flow is negligible compared to that of gravity. Using the procedure of Section 8.2.1, compute the flow rate $q(\varphi,t)$ per unit length along z through a cross-section φ = constant as a function of $h(\varphi,t)$ and the viscosity ν. Both h and q are assumed to remain independent of z. Show that the equation governing the variation of the thickness $h(\varphi, t)$ is: $\partial h/\partial t = -gh^2/(3\nu R)\,(3\partial h/\partial\varphi \sin\varphi + h\cos\varphi)$. Neglecting surface tension effects, compute, for a constant viscosity ν, the variations $h(\varphi, t)/h_0$ at the top and the bottom of the tube ($\varphi = 0$ and $\varphi = \pi$), using the characteristic flow time constant $\tau_f = 3\,\nu R/\left(2\,g\,h_0^2\right)$. Compute then $h(\varphi,t)/h_0$ for $\varphi = 0$ and $\varphi = \pi$ when ν increases exponentially with time as $\nu = \nu_0 \exp(t/\tau_d)$ (in order to simulate the drying of the paint). What is the thickness variation at times short or long compared to τ_d depending on the relative values of τ_d and τ_f?

2) **Spin coating**

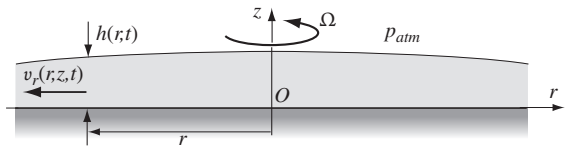

In the "spin coating technique", in order to obtain a thin layer of constant thickness of viscous fluid an initially thicker layer is placed over a horizontal disk rotating at a constant angular velocity Ω around the z-axis. Neglecting surface tension and gravity, show that the flow rate $q(r)$ through a cylinder of radius r and axis Oz, higher than the maximum of the thickness $h(r, t)$ of the layer, is $q(r) = 2\pi\left(\Omega^2 r^2 h^3(r,t)\big/3\nu\right)$. Write the relation between $\partial h/\partial t$ and q and show that, if $h(r, t)$ is constant with r at a time t, it remains so thereafter. What is then the variation $h(t)$ for an initial thickness h_0? What is the thickness after 10 s and 100 s for $\Omega = 60\ \pi$ rad/s, $\nu = 10^{-5}$ m^2/s and $h_0 = 0.5$ mm?

3) **Rough sphere dropping away from a plane**

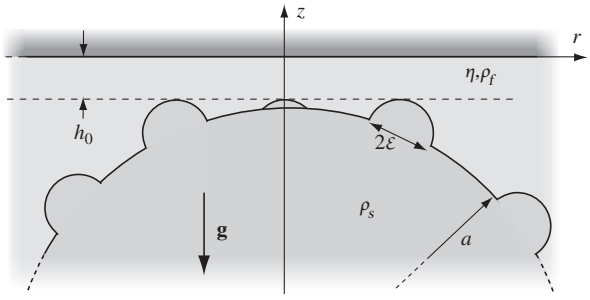

We generalize the analysis of Section 8.1.6 to a rough sphere of radius a. The roughness is represented by a distribution of half spheres of radius $\varepsilon \ll a$. The space between the sphere and the plane is filled by a Newtonian liquid. In contrast to the case of Figure 8.4, the rough sphere is initially below the plane and in contact with it (we assume that three of the small half spheres are at an atomic distance $h_0(0) = h_{0m} \ll \varepsilon$ from the

plane); the sphere moves away under its weight thereafter. Due to the reversibility of low Reynolds number flows, the flow velocity field is the opposite, for a same distance from the plane, of that for a sphere falling towards it. In the early phase of the motion during which $h_0 \ll \varepsilon$, how should equation 8.33 be modified? What becomes of the equation when $\varepsilon \ll h_0 \ll a$? At larger distances $h_0 > a$, equations 8.33 must be replaced by the empirical expression $F = -6\pi\,\eta\,a\left(1 + \frac{a}{h_0}\right) \mathrm{d}h_0/\mathrm{d}t$. Show that it is valid for a sphere with smooth walls both for $h_0 \ll a$ and $h_0 \gg a$. Show that the equation of motion of the sphere is then $\frac{4\pi}{3}\,a^3(\rho_s - \rho_f)g = 6\pi\,\eta\,a\left(1 + \frac{a}{h_0(t)+\varepsilon} + \frac{3\varepsilon^2}{a\,h_0}\right)\frac{\mathrm{d}h_0}{\mathrm{d}t}$ and that the distance $h_0(t)$ satisfies the implicit relation:

$$\frac{2a^2}{9\eta}(\rho_s - \rho_f)t = h_0(t) - h_{0m} + a\,\mathrm{Log}\frac{h_0(t)+\varepsilon}{h_{0m}+\varepsilon} + \frac{3\varepsilon^2}{a}\mathrm{Log}\frac{h_0(t)}{h_{0m}}.$$

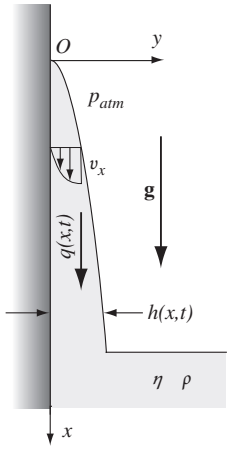

We want to use this equation in order to determine the relative roughness ε/a of the sphere by measuring the times t_a and t_{2a} for its move away by distances a and $2a$ from the plane (J.R. Smart and D.T. Leighton, 1989). Show that ε/a can be written as a function of solely t_a and t_{2a}.

4) **Liquid film draining under gravity along a vertical plate**

A vertical plate ($y = 0$) is dipped into a viscous fluid and then quickly pulled out: it carries with it a layer of fluid of thickness $h(x, t)$ ($x = 0$ at the top of the layer) which drains down due to gravity (surface tension is neglected). Compute the flow rate q per unit length along z through a section x = constant (see Section 8.2.1). Show that, because of the conservation of mass, $h(x, t)$ satisfies the relation $\partial h/\partial t + (g/\nu)\ h^2(\partial h/\partial x) = 0$. We assume that, after a transitory phase, the variation of h corresponds to a self-similar solution: $h = f(x/t^\alpha)$. Determine α and the function f. What is the corresponding thickness of the film at a distance $x = 0.2$ m for $\nu = 10^{-3}$ m^2/s and $t = 1$, 10, 100 and 10^4 s?

5) **Rayleigh-Plateau instability on a cylindrical fiber**

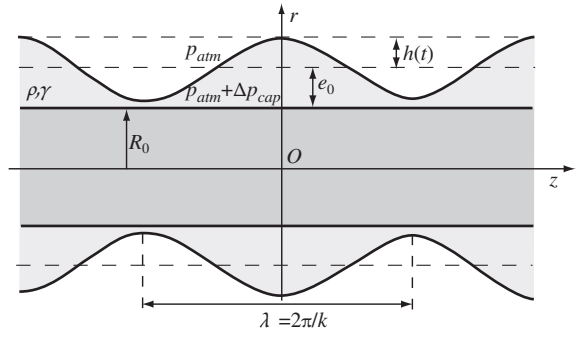

We examine the instability of a viscous film of initially constant thickness e_0 upon a horizontal cylindrical fiber of radius $R_0 \gg e_0$ and axis z. Surface tension and viscosity effects are taken into account while gravity is neglected. The flow along the film is supposed to be quasi-stationary and controlled by viscosity as in Equation 8.25 and not by inertia as in Section 8.3.2. Assuming a sinewave distorsion of the interface ($e(z) = e_0 + h(t)\cos k\,z$) and using a relation similar to Equation 8.86, compute the

pressure $p(z)$ and show that the flow rate $Q(z)$ through a cross-section z = constant is $Q(z) = \left[2\pi\gamma k h e_0^3/(3\eta R_0)\right](k^2R_0^2 - 1)\sin kz$. Using this result, write the conservation of mass at a distance z and show that the governing equation for $h(t)$ is $1/\tau(k) = (1/h)\ (dh/dt) = \left[(k^2 e_0^3\ \gamma)/(3\ \eta\ R_0^2)\right]\ (1 - k^2R_0^2)$. For what value of k does $\tau(k)$ reach its minimum value $\tau_{\min}$? Using the results of Exercise 1, what is the condition on $\tau_{\min}$ which must be satisfied by $\tau_{\min}$ in order for gravity to be negligible, as assumed above? Compute $\tau_{\min}$ and the corresponding wavelength for $\eta = 10^{-1}$ Pa.s, $\gamma = 5 \times 10^{-2}$ N/m, $R_0 = 0.5$ mm and $e_0 = 20\ \mu$m.

6) **Liquid film rising due to the Marangoni effect (Section 8.2.4)**

A vertical plate ($x = 0$) is dipped into a liquid bath of horizontal free surface at $z = 0$. A vertical temperature gradient $\partial T/\partial z < 0$ is established on the plate at the origin time $t = 0$. It creates a vertical gradient $\partial\gamma/\partial z = -b\gamma\ (\partial T/\partial z)$ of the surface tension which causes a liquid film of thickness $h(z, t)$ to move up on the plate. Determine the velocity profile $v_z(x)$ as a function of h and show that the local flow rate q per unit distance along y is $q = \sigma^{(\gamma)}\ (h^2/2\eta) - \rho g\ (h^3/3\eta)$. What is the value of the stress $\sigma^{(\gamma)}$ on the surface? As the film rises, the point where the thickness h has a given value also moves. Show that its velocity V is equal to $\mathrm{d}q/\mathrm{d}h$ and that it is constant with time and depends only on h (use the equation of conservation of mass to relate the variations of q and h). What is the geometrical transformation leading from the profile $h_1(z)$ at a time t_1 to $h_2(z)$ at the time t_2 ? Show that the variation $V(h)$ of the velocity with h displays a maximum. What are the corresponding thickness h_{max} and velocity $V(h_{max})$? Assuming that $h > h_{\max}$ for $z = 0$, explain qualitatively why the profile must be cut off (h goes abruptly to zero) for a value of h which must be larger than h_{max}.